KfK 3409
November 1982

Strain Induced Martensitic Transformation in ZrNbAl TRIP Effect

J. C. Bolcich
Institut für Material- und Festkörperforschung

Kernforschungszentrum Karlsruhe

KERNFORSCHUNGSZENTRUM KARLSRUHE

Institut für Material- und Festkörperforschung

KfK 3409

STRAIN INDUCED MARTENSITIC TRANSFORMATION IN ZrNbAl TRIP EFFECT

J.C. Bolcich[+]

This investigation was performed with technical support by Kernforschungszentrum Karlsruhe under the framework of the German-Argentine Cooperation agreement

Kernforschungszentrum Karlsruhe, GmbH., Karlsruhe

[+]Centro Atómico Bariloche, Instituto Balseiro
Comisión Nacional de Enerîa Atómica and
Universidad Nacional de Cuyo
8400 - S.C. de Bariloche, Argentina

Kernforschungszentrum Karlsruhe GmbH
ISSN 0303-4003

Abstract

A description of possible effects like pseudoelasticity and TRIP, associated with martensitic transformation under applied external stress is given. Related to them, an overview of metastable phases in the zirconium-niobium system is reported.

For this work, deformation experiments under tension and compression in the temperature range between -193°C and 100°C were performed. They reveal the existence of a TRIP effect in the Zr-8wt%Nb-1wt%Al alloy, while no pseudoelastic behaviour is present. The maximum amount of TRIP effect appearing between -54°C and 50°C, corresponds quite well with the higher amount of strain induced martensite plates observed with optical microscopy. An analysis of the fracture zones with scanning electron microscopy, shows always a typical ductile fracture.

Spannungsinduzierte Martensitumwandlung beim
ZrNbAl TRIP-Effekt

Zusammenfassung

Eine Beschreibung möglicher Effekte, die mit der martensitischen Umwandlung unter angelegter äußerer Spannung zusammenhängen, wie Pseudoelastizität und TRIP wird vorgenommen. In Verbindung damit wird ein Überblick über die metastabilen Phasen im System Zirkonium-Niob gegeben.

Für diese Arbeit wurden Zug- und Druckversuche in einen Temperaturbereich zwischen -193°C und 100°C durchgeführt. Sie bestätigen das Vorhandensein eines TRIP-Effektes in der Zr-8Gw%Nb-1Gw%Al-Legierung, während kein pseudoelastisches Verhalten beobachtet wird. Der größte Anteil an TRIP-Effekten, der zwischen -54°C und 50°C auftritt, stimmt gut mit dem höheren Anteil an dehnungsinduzierten Martensitplatten überein, wie er in der lichtmikroskopischen Untersuchung gefunden wird. Eine Untersuchung der Bruchflächen mit Hilfe der Rastermikroskopie zeigt in allen Fällen duktiles Bruchverhalten.

INDEX

1.	Introduction	1
2.	Effects associated with the martensitic transformation. Pseudoelasticity and TRIP effect.	2
2.1.	Pseudoelasticity	2
2.2.	TRIP effect.	3
3.	Binary Zirconium-Niobium system	6
3.1.	Metastable phases in the Zirconium-Niobium system.	7
3.1.1.	Martensite start temperature M_s	8
3.1.2.	Stress and strain induced martensitic transformation	9
4.	Ternary Zr-Nb-Al alloy	12
5.	Sample preparation	12
6.	Experimental results	13
6.1.	Deformation tests	13
6.1.1.	Tension tests	14
6.1.2.	Compression tests	15
6.2.	Optical microscopy	17
6.3.	Scanning electron microscopy	18
7.	Discussion of results	19
7.1.	Tension tests	19
7.1.1.	Relation between σ_y (normal yield stress of the matrix phase) and σ_c (critical stress for the beginning of the strain induced martensitic transformation).	24
8.	Conclusion	25
References		27
Tables		31
Figure captions		41

1. INTRODUCTION

Several studies on steels, specially Fe-Ni, have shown the possibility of having martensitic transformations during plastic deformation, increasing the interest of some investigators for its technological implication like a TRIP effect (67ZAC)(71GER)(70BOL)(71RIC).

With the same aim, previous work on a Zr-Nb-Al alloy was carried out (80 BOL). A martensitic transformation was found to take place while deforming the material at liquid nitrogen and at room temperatures.

The main object of the present work is to probe in a Zr base ternary alloy, the existence of a stress assisted or strain induced martensitic transformation with the corresponding associated effects such as pseudoelastic or TRIP respectively. This would be of interest for developing components to be used in PWR or BWR nuclear core reactors.

Experimental results on deformation which have been performed at different temperatures between -193 and 100°C are presented, including an analysis of the morphology and amount of plates formed at each temperature, and also observations of the fractured zone and the TRIP effect.

2. EFFECTS ASSOCIATED WITH THE MARTENSITIC TRANSFORMATION. PSEUDOELASTICITY AND TRIP EFFECT

2.1. Pseudoelasticity:

This property can be obtained by:

a) a stress induced martensitic phase transformation

b) a reorientation of existing martensite plates

The first case occurs when an alloy in a metastable state and susceptible to undergo a martensitic transformation is stressed at a constant temperature T_1 and when it is possible to obtain a stress-strain curve like that schematically shown in Fig. 1. A neccesary condition, is that T_1 be higher than A_f, where A_f is the temperature at which the inverse transformation (retransformation) is completed without the application of stress. In this figure, the interval AB represents the pure elastic deformation of the matrix phase. Point B, corresponds to a value $\sigma_{T_1}^{P-M}$ for the applied stress at which the first martensite plates start to form. At point C, the transformation is complete. The slope of the interval BC, indicates the facility with which the martensitic transformation takes place. On increasing the applied stress the material which is totally transformed at C will continue its elastic deformation, as is shown by the interval CD of the curve. At point D, plastic deformation of martensite begins and will continue until fracture. If the application of stress is released before reaching point D, for example at point C', the deformation will be recovered in several stages.

The martensitic retransformation starts at point F which corresponds to a $\sigma_{T_1}^{M-P}$ stress, the martensite fraction decreasing up to point G at which the matrix phase is the only one present.

The interval GH represents the elastic unloading of the matrix phase. The deformation may not be recovered to completion, depending on whether irreversible deformation took place or not during loading or unloading of the material. The difference between the stress $\sigma_{T_1}^{P-M} - \sigma_{T_1}^{M-P}$, determines the stress hysteresis of the transformation. The area encircled by the loading and unloading curves gives the amount of energy dissipated during the cycle.

The second case may occur in some alloys such as brasses.

The application of stresses on a material completely transformed into the martensitic phase can produce a "polarization" in the orientation of the plates initially distributed in different directions. This gives a stress-strain curve similar to that shown in Fig. 1 (74KRI).

2.2. Trip effect

It may appear, in an alloy; in which the high temperature beta phase is retained on quenching and in which, due to plastic deformation, a strain induced martensitic transformation occurs afterwards. In general, this effect allows for an apreciable amount of plastic deformation, the materials behaving as ductile but nevertheless showing a high degree of hardening and a high ultimate tensile strength.

Different relationships among applied stress, plastic deformation and martensitic transformation, have been studied by Bolling and Richman (69BOL)(70BOL)(71RIC) in Fe-Ni-C and Fe-Ni-Cr-C alloys. They defined the following characteristic stresses and temperatures, also employed by Olson and Cohen (72OLS), schematically represented in Fig. 2.

M_s is the spontaneous transformation temperature. This is a temperature at which the alloy will transform martensitically on cooling without the application of stresses.

M_s^σ is a temperature, such that: below M_s^σ, the plastic deformation will be produced by the beginning of martensite formation and above M_s^σ, the plastic deformation will be produced by the regular matrix phase slip. It must be noted that below M_s^σ plastic deformation can occur in the matrix and/or the martensite plates, as can also happen in the spontaneous transformation. Above M_s^σ, the critical stress for strain inducing martensite, coincides with the yield stress σ_y at that temperature (7.1.1.). Likewise, the yield stress as a function of temperature, has a negative slope above M_s^σ, while in the range between M_s and M_s^σ the slope is positive. In the second case, when reaching the M_s temperature the stress for inducing martensite tends to zero.

M_d is a temperature, above which the transformation can no longer occur, because the chemical driving force is too small (it can also be zero or negative, depending on M_d being equal to or higher than the T_o temperature, where the free energies of the ß and α' phases coincide). Then,

the product $\sigma.\varepsilon$ added to the free energy change, is not large enough for producing the transformation due to the decrease on the σ-value for higher temperatures. Thus, for this temperatures a smaller incidence of the mechanical term is obtained.

At temperatures below M_s, the deformation that accompanies the martensitic transformation, takes place at lower stresses than the "normal" yield stress (σ_y) of the alloy in the matrix phase that results on extrapolating from higher to lower temperatures.

In this range, the "yield" stress as a function of temperature obeys a law in agreement with the behavior of M_s relative to the elastic applied stress.

Under these conditions we say that the formation of martensite is stress assisted.

Above M_s^σ, the applied stress must reach and may be overcome the σ_y value (yield stress of the matrix phase at that temperature) to allow for the beginning of martensitic transformation.

It can be observed that in the range M_s^σ-M_d, where plastic deformation occurs, the stresses are significantly lower than those resulting from extrapolation of the linear section on the range M_s-M_s^σ. This implies that the mechanisms for martensite formation operative in each range are different. In the first case, the "previous" plastic deformation of the matrix phase introduces new places where martensite plates can nucleate and grow. Thus in the range M_s^σ-M_d, we refer to <u>strain induced</u> martensitic transformation.

3. BINARY ZIRCONIUM-NIOBIUM SYSTEM

Martensitic transformation by quenching: In pure zirconium and diluted zirconium alloys, up to 0,8% Nb in weight, a massive martensite morphology, is obtained. The plates appear dislocated and without internal twinning.

In alloys with compositions between 0.8 and 7% of Nb in weight, acicular internally twinned martensite plates, are obtained. On the primary plates the twinning plane is a $(10\bar{1}1)$ type, while secondary plates appear without twinning (71 BAN).

These authors found that more than one lattice invariant shear system is operative during the transformation, these are the $(10\bar{1}1)$ and $(11\bar{2}2)$ type twinning planes and $(1\bar{0}11)$ type slip plane. From trace analysis, they measured for pure zirconium a $(334)_{\beta}$ type habit plane.

The orientation relationship between matrix and martensite plates, determined with X-ray diffraction techniques (34 BUR) results in:

$$(110)_{\beta}//(0001)_{\alpha} \quad ; \quad (111)_{\beta}//(11\bar{2}0)_{\alpha} \qquad \text{(Fig. 3)}$$

The same crystallographic correspondence, was corroborated by (59 GAU) and (71 BAN).

The principal lattice deformation, comprises a 1.2% expansion along a $(011)_{\beta}$ direction which is transformed into a $(0001)_{\alpha}$; a 10% expansion along another $(0\bar{1}1)_{\beta}$ direction which is transformed into a $(01\bar{1}0)$ and a 10% contraction along a (100) direction which is transformed into a $(2\bar{1}\bar{1}0)$ direction. The

expansion along (011) is small, while the principal deformations along the other two axes are positive and negative, hence the lattice invariant shear nearly corresponds to an invariant plane deformation (34 BUR).

The mechanism of the transformation involves a principal deformation shear on a $(1\bar{1}2)$ type plane of the cubic lattice along a $(\bar{1}11)$ direction and finally a shuffling of atoms in each (110) intermediate plane (Fig. 4).

3.1. Metastable phases in the Zirconium-Niobium system

Depending on the alloy composition (Fig. 5) after quenching from the beta (bcc) phase to room temperature, it is possible to obtain the following:

a) Martensite for compositions between 0 and 7wt% of Niobium:
   For pure Zr, it is not yet clear whether martensitic transformation takes place on cooling at very high rates (65 MCM).
   The upper Nb limit above which it is not possible to obtain martensite by quenching depends on the amount of oxygen, greater Nb concentrations being necessary for high O contents ($\sim$1000 ppm).

b) For compositions between 7 and 20wt% of Niobium, the beta phase is retained and a new precipitated omega phase appears.

c) For compositions of Niobium higher than 20wt%, only beta phase is retained.

3.1.1. Martensite starting temperature M_s

There is no complete experimental agreement among the different authors, concerning the M_s temperature. McMullen and Parr (65 MCM), using zirconium iodide and alloys with 1; 2.5; 3 and 5% in weight of Nb, measured the M_s temperature with cooling rates up to 10.000° C/sec. Higgins and Banks (66 HIG), made measurements in 2.5% wt Nb alloys and an oxygen content between 400 and 700 ppm. Also, Hunt and Niesen (71 HUN), employing alloys with a Nb content between 0,5 and 5,7% in weight and different oxygen amounts between 1420 and 5320 ppm. and cooling rates in the range 50 to 2000 C/seg. determined the Ms temperature.

Among their results there exists an acceptable agreement getting a linear decrease of M_s with the increase of Nb content, obtaining M_s=830°C for pure zirconium and M_s=460°C for Zr-5.7%Nb (Fig.6). It seems that different cooling rates and oxygen contents do not influence the M_s values.

Why does in general M_s decrease? : The temperature M_s decreases with the increment of alloying elements. This tendency is connected with the variation of T_o with composition (T_o is the temperature for which the internal free energy (Gibbs) of the parent and martensitic phase are equal). The "driving force" resulting from the difference between T_o and M_s is a necessary condition for the transformation to occur for balancing and overcoming the non-chemical energies.

3.1.2. Stress and strain induced martensitic transformation:

By means of thermomechanical treatments it is possible to improve the mechanical propertie of zirconium alloys without the need of excessively increasing the amount of alloying elements. A method may consist of a strain induced martensitic transformation by deformation from a metastable beta phase to a martensitic α'_D phase.

Delvecchio et al. (69DEL)(70DEL)(71DEL) worked initially in Zr-3wt% Mo alloys looking for a strain induced martensite. The mechanical behaviour of this alloy was brittle, maybe due to the presence of omega precipitates. The addition of 1wt% Aluminum, increases the stability of beta phase relative to that of the omega phase and reduces it relative to that of the strain induced martensitic phase α'_D when deforming by rolling at room temperature. According to their results, the addition of aluminum inhibits the formation of omega after quenching. They supposed that it is possible that the size of Aluminum atoms play an important role on the coherency of deformations and short range diffusion associated with the formation of omega (70DEL).

The α'_D plates are nucleated at grain and/or twin boundaries extending through well defined crystallographic directions. According to variations of the lattice parameters in the α'_D phase those authors suggested that regions of the β phase that are deficient in beta stabilizer transform initially to α'_D. Electrical resistivity measurements on the stressed samples show that the biggest amount of transformation takes place in the first stages of deformation.

The α'_D phase shows an hcp structure similar to that of the equilibrium α phase.

The orientation relationships between the beta matrix and martensitic α'_D phase are those reported by Burgers (Fig. 3).

Delvecchio et al. (71 DEL) found a morphology and amount of strain induced martensite strongly dependent on the testing temperature. On decreasing temperature down to -196°C they got an increase in the amount of transformation with respect to that obtained by deforming at room temperature. The morphology is similar, consisting in plates oriented along well defined crystallographic directions. By rolling at 200°C a small amount of martensite appears while the morphology is similar to a "spider-web" with smaller plates size than that induced at liquid nitrogen temperature. Marques (78 MAR) studied different alloys of Zr-3at% Mo with variable amounts of Al, La and Ti. He found strain induced martensite depending the morphology and amount of transformation on testing temperature. At lower temperatures, the plates are shorter and thinner. The martensite shows a $(334)_\beta$ type habit plane and fits well with the Burgers orientation relationships. The internal substructure appears highly faulted and twinned. No dislocations were observed in the no transformed beta matrix as in the martensite plates α'_D.

Northwood and Rezek (72 NOR) proposed a stability diagram for predicting the mode of deformation to be produced in an alloy (Fig. 7). This diagram was initially proposed by Rack

et al. (70RAC) for Titanium alloys. They employed an alloy of Zr-0,8% Mo-2% V-2% Nb- 2% Sn in weight with small variations in the different alloying elements.

They pointed out that because Mo is a highly beta stabilizing element it is very important to control its content in those alloys that present a favourable behaviour for mechanical processing. A Mo excess can modify the effective composition towards regions out of region 1 where it is not possible to produce a strain induced transformation. The Nb appears as a less effective beta stabilizer, whereas Al and Sn behave as alfa stabilizers with Al presenting a more pronounced effect than Sn.

Table N° 1 shows a list of alloys employed by different authors that present a strain induced martensitic transformation. The amount of transformation is shown in some cases. In general, there is good agreement among different investigators except for the Zr-3wt% Mo alloy for which (72 NOR) did not find any transformation, while on the other hand (78 MAR) showed abundant.

For Zirconium alloys with compositions such that beta phase is retained after quenching, (59 GAU) tried to produce strain induced martensite without any success. (80 BOL) using Zr-(8-10) wt % Nb tried to obtain strain induced martensitic transformation in quenched alloys. The retained ß phase plus omega precipitates made a very brittle material when tested at different temperatures. Rupture was reached before getting a martensitic phase transformation.

4. TERNARY Zr-Nb-Al ALLOY

For zirconium, elements with valence higher than 4 are beta stabilizers whereas those with valence less than 4 are α stabilizers (Table 2). By adding ~ 1 wt% of Al to Zr-8wt% Nb alloys, it is possible to have a stress induced martensitic transformation (80BOL).

With the purpose of getting insight into mechanical parameters associated with this behavior, samples with nominal compositions of Zr-8 wt% Nb-1 wt% Al were prepared and tested at temperatures between -193°C and 100°C.

5. SAMPLE PREPARATION

a) Melting: samples of Zr-8wt% Nb-1wt% Al alloys were melted in an arc furnace with a non consumable tungsten electrode and a water cooled copper crucible in a high purity inert argon gas atmosphere (70LEY)(77HOL)(78BOL)(80DEN).

This process involves two stages:

i) melting of the alloy in order to get a final "button" geometry.

ii) remelting the alloy into a rod. This process is performed in a horizontal crucible with semi-cylindrical cross section.

b) Machining: to the geometry shown in Fig. 8(a) for tension probes and to rods of 3 mm diameter and ~10 mm length for compression probes.

c) Thermal treatment: In order to retain the high temperature beta phase, the samples are encapsulated (in vacuum after two or three times argon purging) into sylica tubes and are water quenched from 1000°C by breaking the capsule.

6. EXPERIMENTAL RESULTS

6.1. Deformation tests

Employing an INSTRON, Model TT-type D, Universal testing machine, tension and compression tests were performed in the temperature range (-193°C to 100°C).

In all cases the velocity of deformation was of 0.5 mm/min. The elongation was measured by means of an electromechanical extensometer, one end fixed to the crosshead and the other end to the frame of the deformation machine.

In Table 3 are indicated the different probes employed, being their nominal composition Zr-8% Nb-1% Al in weight.

By metallographic techniques, it was verified that before deformation the initial phase of the samples was beta (bcc). It was also determined that no strain induced martensite had appeared during machining, (very thin steps of the order of 0.1 mm were used).

6.1.1. Tension tests

The geometry of the samples is shown in Fig. 8.a. The ends are threaded in a length of 10 mm. (RM 0.7-4 mm diameter); the central part is cylindrical with 3 mm diameter and 20 mm length. For metallography, the different zones of the samples were called B(Bruch), M(Medium) and K(Kopf).

The load-elongation curves, for temperatures of 100, 50, 0, -54, -101 and -193°C are shown in Figs. 9(a); 9(b), 9(c), 9(d), 9(e), 9(f), respectively.

In all the measurements, cycles of load-unload were performed in order to determine whether a pseudoelastic effect appears or not for that temperature and amount of deformation. This effect was not observed in any test. On completely unloading the material a plastic deformation equivalent to that obtained on loading is still present in the sample (only the elastic range was recovered). In another loading run the curve followed the same variation as in the unloading one.

The value of tension relative to the initial cross-section of the sample (the so-called true tension), the engineering deformation $\varepsilon_t = \ell n \frac{\ell}{\ell o}$ and the linear deformation $\varepsilon'_f = \frac{\Delta \ell}{\ell o}$ were calculated for each curve, taking into account the constant volume condition during plastic deformation.

All these data are given in tables N° 4/1 to 4/6 respectively, where:

ℓ is the length of the sample on the measured point of the load-elongation curve.

ℓ_o is the initial length of the sample.

The critical yield stress (σ_c) as a function of temperature is given in Fig. 10 where a monotonous decreasing behaviour is observed on increasing T (°C). This behaviour is similar to that of the yield stress for plastic deformation. Both tension values σ_c and σ_y (7.1.1.) are the same for a given temperature.

The ultimate tensile strength σ_{UTS} and the plastic deformation calculated as linear deformation are represented as a function of temperature in Fig. 11.

6.1.2. Compression tests:

Using cylindrical samples of 3 mm diameter and 7.5 mm length, compression tests up to rupture were performed at the following temperatures:

112 ; 90 ; 60 ; 30 ; 0 ; -23 ; -49 ; -58; - 86 ; -193 °C.

The load-elongation curves are similar to those obtained in the tension tests, some of them with characteristic features of the mode of deformation which are discussed below.

For each temperature the values of yield stress (σ_y), ultimate tensile stress σ_{UTS}, plastic deformation up to rupture ε'_f and hardening coefficient n, were determined.

The results exihibit the same behaviour as a function of temperature as those of the tension test. A greater dispersion is observed, however, which can be due to a lack of parallelism between the transverse surfaces on the samples that rest on the

compression plates of the deformation machine and also, to the stresses developed at the ends of the samples.

Comparing those measurements, we can assert:

-- The yield stress is smaller at temperatures below 0°C and greater at higher temperatures.

-- The ultimate tensile strength obtained by compression is higher than that obtained by tension in all the temperture range.

-- The deformation up to rupture is approximately twice of that obtained by tension.

-- The hardening coefficient n as a function of the testing temperature or the amount of deformation behaves in a similar way, it is very significative at temperatures higher than -50°C and negligible in the low temperature range (-101; -193°C). This coefficient is smaller at the beginning of plastic deformation and at higher temperatures appears a kind of "easy glide" zone. The width of this zone is greater at higher temperatures.

The fracture in the compression samples, generally occured by sliding on inclined planes with respect to the axis of the sample and at a distance approximately equidistant from the supporting extremes. Also, it is quite difficult to maintain adequate alignment conditions during the whole test. This could explain the higher measured values of σ_y and σ_{UTS}. In each test, cycles of loading-unloading up to different degrees of deformation were performed, a pseudoelastic effect not appearing in any of the tests.

6.2. Optical Microscopy

Micrographs of the samples were taken prior to the deformation tests in order to verify that only the beta phase has been retained. In Fig. 8b a transverse section of a sample with the original beta grains and some isolated strain induced martensitic plates produced by saw cutting can be seen.

A macrophotograph of a sample used for tension test is shown in Fig. 8a.

In Fig. 8c a scheme of the different zones of the sample is shown:

B fracture zone: M medium zone and K head zone. Micrographs of the B, M, and K zones corresponding to the samples deformed by tension at different temperatures are shown in Figs. 12(a) to (f). Other data as number of sample, temperature of deformation and morphology observations are given in Table N° 5. From them it is possible to deduce that with respect to the temperature dependence the greatest amount of strain induced martensite appears in samples deformed between -50 and 50 °C (M and K views), existing a correspondence with the higher amounts of deformation (Fig. 11). In this temperature range, the TRIP EFFECT is highest.

In general, on the fracture zone B there is less amount of plates than in M and K. This could be explained by the fact that the fracture is produced in a region of the sample where the TRIP effect is minor and thus, the amount of martensite plates.

The morphology of the samples tested at lower temperatures (-193°C) consists of a smaller number of variants of strain induced martensite plates which are thinner and longer. This could be due to the fact that this is the most stable configuration at this temperature. Also, it is more difficult for dislocations to move and for the plates to grow.

6.3. Scanning electron microscopy

The samples deformed by tension were observed with scanning electron microscopy, to determine qualitatively the type of fracture presented in these alloys and its dependence with temperature (Fig. 13 a. to j.)

A list of the photographs, number of samples, testing temperatures and morphology observations are given in Table 6.

In the whole temperature range, the fracture is ductile the depth of dimples being larger at higher temperatures showing a more ductile behaviour, as in austenitic steels or in copper (78 MIT). The flat dimples are typical of fracture at lower temperatues. Some microholes are observed. This is an intrinsic problem concerning the fabrication process of the samples. To eliminate them, a high temperature forging process after melting would be necessary.

7. DISCUSSION OF RESULTS

7.1. Tension test

On comparing $\sigma_c = \sigma_y$, σ_{UTS} and ε_f', we found that: At temperatures, lower than -100°C, σ_y differs very little from σ_{UTS} (10% approximately) and the plastic deformation is small (around 4%).

As discussed in point 2.2, it is important to produce a strain induced martensitic transformation for obtaining the TRIP effect. In the plate growth process, it is necessary that the matrix can deform plastically, including in this deformation the possibility of producing new potent sites for nucleation of plates. At lower temperatures, the yield stress of the material is higher (70 to 100 Kgr/mm^2), because the critical stress for moving dislocations is also higher. Then, the alloy is rather brittle, ε_f' is low as was already mentioned and only a moderate formation of martensite plates is produced, consistent with a small TRIP effect.

It is important to remark that in spite of being in the low temperature range closer to the spontaneous transformation temperature M_s which corresponds to a larger chemical "driving force", the martensite plates form less easily. It is not possible to produce either a spontaneous transformation or a stress induced martensite, the possibility of plates to grow being dependent on the facility of dislocations to move and of platic deformation to take place on the material.

At temperatures between -100 and 0°C we observe a sharp increase in the plastic deformation ε_f reaching values as high as 30%. Likewise, σ_{UTS} increases and presents a relative maximum at temperatures around 0°C whereas σ_y decreases monotonously as it would be expected for the behaviour of the yield stress with temperature. In this temperature range, it is easier to move dislocations and consequently, the plastic deformation increases, thus contributing to the process of growing and maybe to the formation of new martensitic nuclei. As the deformation and the multiplication of the martensite plates progress, the alloy hardens. This explains the higher σ_{UTS} value obtained.

A similar behaviour was found between 0 and 50°C. However, on increasing the temperature a decrease in the σ_{UTS} and ε_f values appears whereas σ_y keeps on decreasing but at a lower rate.

We can say that between 50 and 100°C, the temperature is still very far from the spontaneous transformation temperature, the chemical diving force resulting quite saml1. The mechanical term, which is added to the free energy change and is given by the tensorial product between the stress state and the deformation state $\overline{\overline{\sigma}}.\overline{\overline{\varepsilon}}$ is also less significative because σ_y decreases. Then the amount of strain induced martensite is less (TRIP). When the TRIP effect diminishes the plastic deformation consequently decreases. If the temperature is increased still more, only the beta matrix will deform without undergoing a phase transformation. Despite the hardening coefficient $\underline{n}$ is appreciable, (Fig. 14) the σ_{UTS} decreases because of the lower values of σ_y and the lesser amout of TRIP effect.

In Fig. 15, the true stress versus the true plastic deformation curve is represented

$$\sigma = F/A \qquad \varepsilon_t = \ell n \cdot \frac{\ell}{\ell o}$$

where these magnitudes are compared for different testing temperatures.

We can observe that for the tempeatures values of -54; 0; 50 and 100°C, the curve σ vs ε_t consists of three regions:

- A first linear region where the elastic deformation takes place. From the slope of the curves in this region, it can be deduced that elastic deformation took place in the grips and frame rods of the deformation machine. Thus, the analysis we shall make from the different deformation curves in this elastic region, will not totally correspond to the behaviour of the tested samples.
- An intermediate region where the slope is small, which we can call "easy glide".
-- A region where the slope of the curve becomes larger at higher deformations, implying the existence of a hardening process.

For the temperature values of -101 and -193°C, only the first elastic deformation region appears, with the second derivate of σ vs ε_t being slightly possitive. On increasing deformation a narrow zone of plastic deformation with positive slope is present. From the analysis of these curves, we can say:

-- In the elastic region, the second derivative is small and negative for the higher temperatures (50 and 100°C), zero (null) for intermediate temperatures (0 and -54°C) and small with positive value for the lower temperatures (-101 and -193°C).

-- The "easy glide" region is more extended and also with a smaller slope for the 100 and -54°C temperatures.

-- The hardening region presents a higher slope for a temperature of 50°C, decreasing smoothly for a temperature of 100°C and decreasing more for the lower temperatures.

-- From results of deformation on the optical microscope stage (82 BOL), it is known that at the beginning of plastic deformation (starting of the second region), one variant of martensite plate is induced. On increasing deformation the region of "easy glide" will contribute to the growth and the phase transformation process. The width of this region, is larger for the higher temperature values. This indicates that a greater degree of formation is necessary to reach the free energy change that allows the prosecution formation of new variant plates, thus, starting the third region. In this region a hardening effect appears which can be attributed to different variant plates interaction.

At lower temperatures, the material shows a little degree of transformation due to the little feasibility of higher plastic deformation.

The hardening coefficient, can be calculated from the relationships

$$\sigma = k \cdot \varepsilon_t^n; \qquad n = \frac{\varepsilon_t}{\sigma} \cdot \frac{d\sigma}{d\varepsilon}$$

The derivate $d\sigma/d\varepsilon_t$ is calculated as the slope of the tangent line to the curves at each point (Fig. 15) and measuring the corresponding calues of σ and ε_t. The values of $\underline{n}$ as a function of the plastic deformation ε_t are indicated in Table N° 7 taking the testing temperature as a parameter. The values of the slope must be multiplied by a scale factor which results equal to 500 Kgr/mm^2 x $(\Delta cm_\sigma/\Delta cm_\varepsilon)$, from Fig. 13. The values of n vs ε_t are plotted on Fig. 14.

At lower temperatures, -193 and -101°C, n presents a value near unity. At higher temperatures, n decreases stepply presenting a minimum between (0.06 and 0.10). On continuing the deformation n increases. This result, is consistent with the temperature at which the higher TRIP effect appears, which is around 0-50°C (see Optical Microscopy results-6.2.). This means that another variant of martensite starts to appear after a short deformation interval, by interaction with the first one the hardening effect is produced, as can be seen for increasing values of deformation.

For the temperatures of 0; 50 and 100°C, the n coefficient increases, presenting a relative maximum around 0,15-0,18.

In the temperature range where the TRIP effect is higher, an adequate balance of the following parameters may be responsible for it:

- the chemical driving force

- the mechanical component $\sigma.\varepsilon$ which contribute to the free energy change
- the possibility of moving dislocations and thus, deforming the alloy plastically.

7.1.1. Relation between σ_y (normal yield stress of the matrix phase) and σ_c (critical stress for starting and strain inducing martensitic transformation).

In the plot of n vs plastic deformation, we found only one peak. In Fe-Ni two peaks (81 KOB) can appear, one corresponding to the initial plastic deformation and hardening of the matrix phase and the other due to the TRIP effect.

Another important fact is that from experiments of deformation on the optical microscope stage (82 BOL), the starting of plastic deformation coincides with the appearance of a martensite plate variant. All these results will be compatible if σ_y coincides with σ_c. If two peaks existed (n vs ε) the following relationship should be fulfilled: $\sigma_y < \sigma_c$.

On the other hand, if σ_y were greater than σ_c, the functional dependence of stress vs temperature should give a positive derivative, but the opposite behaviour is observed.

Finally, the condition of $\sigma_y \equiv \sigma_c$ is fullfilled. Another argument in favour of this condition, is the relatively high value of the measured macroscopic shear (~11%) (82BOL) and the appearance of only one martensite variant at the beginning of

plastic deformation. Both phenomena, imply that the matrix must deform plastically, simultaneously to the strain induced martensitic transformation.

8. CONCLUSIONS

According to our results, we state that the TRIP effect which is present in the Zr- 8w%Nb-1wt%Al considerably improves its mechanical properties. High values of ultimate tensile strenght σ_{UTS} together with a high plastic deformation and a ductile fracture results.

The critical stress σ_c for starting the strain induced martensitic transformation is equivalente to the yield stress σ_y or critical stress for moving dislocations.

The limiting factor in the attainable degree of strain induced martensitic transformation α'_D is the growth of plates which depends on dislocation movility rather than on the chemical driving force. This means that even though the temperature is decreased below T_0, a higher degree of transformation is not necessarily achieved. No pseudoelastic effect was found in this alloy.

The reported σ_{UTS} and strain to rupture values, can be improved by:

a) eliminating the microvoids and controlling size and distribution of grains, by means of high temperature forging.
b) Optimization of the gas content in the alloy, which makes solid solutions hardening.

ACKNOWLEDGEMENTS

The author wish to express his gratitude to Profs. M. Boček (KfK) and M. Ahlers (Centro Atómico Bariloche, CNEA, Argentina) for their very helpful suggestions and discussion of results, to Ing. H. Schneider and Mr. C. Petersen for their collaboration with the deformation experiments and constant encouragement during the course of this works. Thanks are also due to Mr. G. Schanz and Mrs. B. Kammerichs for metallographic examination and to Lic. E.H. Toscano (At this time on leave from Centro Atómico Constituyentes, CNEA, Argentina, in KfK) for the scanning electron microscope observations.

The author is grateful to Adela Abu Arab for providing assistance with the English manuscript.

References

(34BUR) Burgers, W.G., Physica, 1, 561 (1934). "On the process of transition of the cubic-body-centered modification into the hexagonal close-packed modification of Zirconium".

(59GAU) Gaunt, P. and Christian, J.W., Acta Met., Vol.7 (1959) 534. "The crystallography of the ß→α transformation in Zirconium and in two Titanium-Molybdenum alloys".

(65MCM) McMullen, A.G. and Gordon Parr, J., Canadian Metallurgical Quarterly 4, N° 2, 117 (1965). "The transformation in Zirconium-Niobium alloys".

(66HIG) Higgins, G.T. and Banks, E.E., Brit.J.Appl.Phys. 17 (1966) 283. "The martensite start temperature in dilute Zr-Nb alloys".

(67ZAC) Zackay, V.F., Parker, E.R., Fahr, D. and Busch, R., Trans.ASM 60 (1967) 252.

(69BOL) Bolling, G.F. and Richman, R.H., Phil.Mag. 19 (1969) 247. "The plastic deformation of ferromagnetic fcc Fe-Ni-C alloys".

(69DEL) Delvecchio, G.A., Thesis: Faculty of Graduate Studies, University of Windsor, 1969, Canadá. "The strain induced transformation in Zircoium base alloys, and its effect on mechanical properties".

(70BOL) Bolling, G.F. and Richman, R.H., Scripta Met. 4, (1970) 539. "The influence of stress on martensite-start temperatures in Fe-Ni-C alloys".

(70BOL) Bolling, G.F. and Richman, R.H., Acta Met. 18 (1970) 673. "The plastic deformation-transformation of paramagnetic fcc Fe-Ni-C alloys".

(70DEL) Delvecchio, G.A., Northwood, D.O. and Rezek, J., Journal of Nuc.Mat. 35 (1970) 67. "The influence of Al on the stability of quenched ß Zr-Mo".

(70LEY) Leyt, A., Informe CNEA TE 3/41 (1970). "Los procesos de fusión por arco de metales reactivos".

(70RAC) Rack, H.J., Kalish, D. and Fike, K.D., Materials Sci.Eng. 6 (1970) 181. "Stability of As-quenched beta III-Titanium alloy".

(71BAN) Banerjee, S. and Krishnan, R., Acta Met., Vol.9 (1971) 1317. "Martensitic transformation in Zr-Nb Alloys".

(71DEL) Delvecchio, G.A., Northwood, D.O., Osborne, D.E. and Rezek, J., Journal of Nuc.Mat., 38 (1971) 121. "The strain induced martensitic transformation in Zr-3Mo-1Al".

(71GER) Gerberich, W.W., Hemmings, P.L. and Zackay, V.F., Met. Trans. 2 (1971) 2243. "Fracture and Fractography of Metaestable Austenites".

(71HUN) Hunt, C.E.L. and Niessen, P., J.Nuclear Mat., 38 (1971) 17. "The continuous cooling transformation behaviour of Zirconium-Niobium Oxygen alloys".

(71RIC) Richman, R.H. and Bolling, G.F., Met.Trans.2 (1971) 2451. "Stress Deformation and Martensitic Transformation".

(72NOR) Northwood, D.O. and Rezek, J., Can.Met. Quarterly, Vol.11 (1972) 213. "Microestructural examination of strain induced phase transformation in selected Zr alloys".

(72OLS) Olson, G.B. and Cohen, M., J. of the Less Common Metals 28 (1972) 107. "A mechanism for the strain-induced nucleation of martensitic transformations".

(74KRI) Krishman, R.V., Delaey, L., Tas, H. and Warlimont, H., Journal of Mat. Science 9 (1974) 1536. "Thermoplasticity, pseudoelasticity and the memory effects associated with martensitic transformations".

(77HOL) Holt, B.J., Diaz, J.V., Huber, J.G. and Luengo, C.A., S-026/77. Inst. Físico Gleb Wataglin, Univ.Est. Campinas, Brasil (1977). "A Made in Brazil Metallic Sample Preparation Facility".

(78BOL) Bolcich, J.C. and Peretti, H., VII Reunión AATN, San Rafael (Mendoza) (1978). "Fabricación de aleaciones de Zr-Nb (0-10%) y preparación de probetas de uso de laboratorio".

(78MAR) Marques, F.D.S., Z. Metallkunde, Bd. 69 (1978) H,3; 157. "Deformation - induced transformation in metaestable ß Zr based alloys".

(78MIT) Mitsche, R., Jeglitsch, F., Stanzl St. und Scheidl, H., unter Mitwirkung von G. Pfefferkorn. "Radex Rundschau, Heft 314 (1978), Anwendung des Rasterelektronenmikroskops bei Eisen- und Stahlwerkstoffen".

(78NOR) Northwood, D.O., Journal of the Less-Common Metals, 61 (1978) 199. "Heat treatment transformation reactions and mechanical properties of two high strength Zr alloys".

(79NOR) Northwood, D.O. and Lim, D.T., Can. Met. Quarterly, Vol.18 (1979) 441. "Phase transformations in zirconium and its alloys".

(80BOL) Bolcich, J.C., Peretti, H.A. and Ahlers, M., Journal of Nuclear Materials, 95 (1980) 311-313. "Omega and the martensitic transformation in Zr-10Nb and Zr-10Nb-1Al".

(80DEN) De Nicola, J.M., Práctica final de carrera, Universidad Nacional del Sur, Bahía Blanca, Argentina, 1980.

(82BOL) Bolcich, J.C., Thesis. Instituto Balseiro (CNEA-UNC), Centro Atómico Bariloche (CNEA), 1982, Argentina. "Transformaciones de fase sin difusión en aleaciones de Zr-Nb y Zr-Nb-Al".

TABLE N° 1

STRAIN-INDUCED Transformation after up to a maximum of 30% reduction by rolling at Room Temperature [79NOR].

Alloy composition (wt %)	Amount of transformation. % of ß phase transformed	Reference
Zr-3Mo	--	[70DEL] [71DEL] [72NOR]
Zr-3Mo-1Al	100	[70DEL] [71DEL] [72NOR]
Zr-3Mo-1Sn	30 (before cracking)	[72NOR]
Zr-3Mo-2Sn	10-20	[72NOR]
Zr-1Mo-2Nb-2V-1Sn	30	[72NOR]
Zr-1.3Mo-2Nb-2V-2Sn	--	[72NOR]
Zr-.8Mo-2Nb-2V-2Sn	30 (before cracking)	[72NOR]
Zr-3.2Mo	abundant (amount not given)	[78MAR]
Zr-3.2Mo-0.9Al-0.5La	" " " "	[78MAR]
Zr-4.1Mo-33.2Ti	" " " "	[78MAR]
Zr-3Mo-2Sn	" " " "	[78NOR]
Zr-1Mo-2N-2V-2Sn	" " " "	[78NOR]

TABLE N°2

Effect of Solute Valence on Phase stabilization of Zirconium

Element	Pauling Metallic Valence	Ordinary Chemical Valence	Allotropic Phase stabilized
Sb	1.56	3,5	α
Ge	2.56	4	α
Sn	2.56	2,4	α
Pb	2.56	2,4	α
Al	3	3	α
Y	3	3	α
Gd	3	3	α
Tb	3	3	α
Dy	3	3	α
Ho	3	3	α
Er	3	3	α
Lu	3	3	α
In	3.56	3	α
Hf	4	4	α
Cd	4.56	2	α
Si	2.56	4	-
Zr	4	4	-
Ti	4	4	ß
Th	4	4	ß
Zn	4.56	2	ß
V	5	3,5	ß
Nb	5	3,5	ß
Ta	5	5	ß
Cu	5.56	1,2	ß
Ag	5.56	1	ß
Cr	6	2,3,6	ß
Mo	6	3,4,6	ß
W	6	6	ß
U	6	4,6	ß
Mn	6	2,3,4,6,7	ß
Fe	6	2,3	ß
Co	6	2,3	ß
Ni	6	2,3	ß

TABLE N°3

List of probes used in deformation experiments-compositions

Probe N°	Type of deformation	Test Temperature [°C]	% Zr in weight	% Nb in weight	% Al in weight
1-d	Tension	-54°C	91,23	7,77	1,00
2-d	Tension	100°C	90,92	8,07	1,01
3-d	Compression		90,98	7,99	1,03
4-d	Tension	0°C	91,06	7,94	1,00
5-d	Compression		91,12	7,89	0,99
6-d	Tension	-101°C	90,98	8,02	1,00
7-d	Tension	-193°C	90,99	8,00	1,01
8-d	Tension	50°C	91,23	7,75	1,02
10-d	Compression		91,12	7,87	1,01

TABLE N° 4

Stress and strain calculated values (as indicated) from the experimental load-alongation curves with constant volumen condition.

Column 1: Correlative number of measured point
Column 2: Division between load/transversal area
Column 3: Division between load/true transversal area
Column 4: True plastic deformation
Column 5: Linear plastic deformation

TABLE N° 4-1

Probe N° 2-d Temperature: 100°C
Stress at the end of elastic range: 31.31 kp/mm^2

1	2	3	4	5
2	7.78	7.85	.00783	.00786
3	20.94	21.53	.02540	.02572
4	30.84	32.15	.03839	.03914
5	31.36	33.40	.05987	.06170
6	32.55	35.62	.08654	.09040
7	34.11	37.98	.10352	.10907
8	38.56	43.82	.12334	.13127
9	42.89	49.73	.14305	.15379
10	47.25	55.79	.16057	.17419
11	51.83	62.09	.17433	.19044
12	57.75	70.96	.19895	.22013
13	64.16	80.84	.22305	.24988
14	64.94	82.38	.22965	.25816

TABLE N° 4-2

Probe N° 8-d Temperature: 50°C
Stress at the end of elastic range: 34.00 kp/mm²

1	2	3	4	5
4	10.45	10.55	.00846	.00849
5	18.67	18.99	.01494	.01506
6	27.90	28.64	.02337	.02364
7	34.03	35.15	.02878	.02920
8	34.70	36.56	.04862	.04982
9	39.20	43.12	.09092	.09518
10	48.05	55.05	.13046	.13935
11	55.68	65.39	.15428	.16682
12	66.30	80.44	.18528	.20356
13	71.45	88.46	.20476	.22723
14	76.67	98.09	.23652	.26683

TABLE N° 4-3

Probe N° 4-d Temperature: 0°C
Stress at the end of elastic range: 46.28 kp/mm²

1	2	3	4	5
4	9.47	9.53	.00568	.00570
5	23.77	24.25	.01757	.01772
6	40.95	42.38	.03010	.03056
7	46.85	48.77	.03532	.03596
8	48.63	50.86	.03980	.04061
9	52.00	56.58	.07870	.08188
10	53.25	58.39	.08629	.09012
11	57.29	64.35	.10974	.11599
12	65.12	76.28	.15057	.16249
13	70.41	84.64	.17561	.19197
14	77.46	97.08	.21607	.24119
15	80.19	##.##	.23809	.26882
16	81.77	##.##	.25954	.29634
17	82.18	##.##	.26233	.29995

TABLE N° 4-4

Probe N° 1-d Temperature: -54°C
Stress at the end of elastic range: 60.77 kp/mm²

1	2	3	4	5
2	29.61	30.31	.02035	.02055
3	45.33	46.99	.03124	.03173
4	58.32	61.16	.04145	.04232
5	66.17	70.26	.05299	.05442
6	67.99	73.48	.07029	.07282
7	68.12	75.00	.08872	.09277
8	69.52	78.24	.11039	.11671
9	70.64	80.90	.12752	.13601
10	71.85	83.12	.13737	.14725

TABLE N° 4-5

Probe N° 6-d Temperature: -101°C
Stress at the end of elastic range: 69.40 kp/mm²

1	2	3	4	5
2	9.93	10.01	.00629	.00631
3	30.06	30.75	.01952	.01971
4	53.06	55.17	.03357	.03414
5	69.28	72.95	.04439	.04539
6	73.76	78.32	.05220	.05359
7	74.83	79.94	.05812	.05984

TABLE N° 4-6

Probe N° 7-d Temperature: -193°C
Stress at the end of elastic range: 100.04 kp/mm²

1	2	3	4	5
2	16.07	16.26	.01050	.01055
3	48.25	50.04	.03146	.03196
4	67.89	71.45	.04406	.04504
5	79.45	84.32	.05114	.05248
6	90.52	96.83	.05779	.05949
7	99.54	##.##	.06416	.06626
8	##.##	##.##	.07236	.07594
9	##.##	##.##	.07837	.08152

TABLE N° 5

Optical microscopy observations of samples tested by tension
(Magnification × 100)

Photo N°	Sample	Deformation temperature	Morpholgy observation
12 a	2-d	100°C	B = few plates; M and K = almost complete transformation in all the grains.
12 b	8-d	50°C	B = medium amount of plates, preferentially one variant. M =almost total transformation K = total transformation
12 c	4-d	0°C	B,M,K. = high percentage of transformation, but larger in K.
12 d	1-d	-54°C	B,M,K = high percentage of transformation, but less than at 0°C.
12 e	6-d	-101°C	B,M = transformed area larger than 50%, but less than at -54°C. K = it appears only little isolated plates.
12 f	7-d	-193°C	B = less than 50% of transformation M and K = only little isolated plates. Morphology of plates: thinner than that produced at higher temperatures.

TABLE N° 6

Samples used in Scanning Electron microscopy to observe fractured zone

Photo N°	Sample	Deformation temperature	Observations [78MIT]
13 a	2-d	100°C	Typical ductile fracture structure (dimples), pronounced relief.
13 b	2-d	100°C	Microvoids, produced during melting and solidification of the sample. Some of them, present a zone with teared off material.
13 c	8-d	50°C	Intergranular ductile fracture
13 d	8-d	50°C	Intergranular ductile fracture
13 e	1-d	-54°C	Intergranular ductile fracture (dimples) with less relief
13 f	6-d	-101°C	Intergranular fracture. Some dimples.
13 g	6-d	-101°C	Microvoids with ductile fracture zone and slipped planes.
13 h	6-d	-101°C	Idem 7, with higher magnification
13 i	7-d	-193°C	General view with low magnification. Ductile fracture, larger dimple size.
13 j	7-d	-193°C	Ductile fracture structure (dimples). Little relief. Flat dimples and larger than in samples deformed at higher temperatures.

TABLE N° 7

Hardening coefficient n as a function of the engineering plastic deformation ε_t.

Temperature	ε_t	σ [kgr/mm²]	$d\sigma/d\varepsilon_t$ [α]	$d\sigma/d\varepsilon_t = tg\alpha$ [×500Kgr/mm²]	$n = \frac{\varepsilon_t}{\sigma} \times \frac{d\sigma}{d\varepsilon}$
100°	0.01	10.5	60°	1.73	0.83
	0.02	18	58°	1.60	0.89
	0.03	26	57°	1.54	0.89
	0.04	32,5	10°	0.18	0.11
	0.05	32,7	7°	0.12	0.09
	0.06	33	7°	0.12	0.11
	0.07	34	8°	0.14	0.15
	0.08	35	11°	0.19	0.22
	0.09	36	15°	0.27	0.34
	0.10	37	18°	0.32	0.43
	0.11	37,5	28°	0.53	0.78
	0.12	42	30°	0.58	0.83
	0.13	45,5	33°	0.65	0.93
	0.14	49	37°	0.75	1,07
	0.15	52	38°	0.78	1,12
	0.16	55,5	38°	0.78	1,12
	0.17	58,5	38°	0.78	1,13
	0.18	64	38°	0.78	1,11
	0.19	67	38°	0.78	1,11
	0.20	71	38°	0.78	1,10
	0.21	75	36°	0.73	1,02
	0.22	79	32°	0.62	0.87
	0.23	82	25°	0.47	0.66
50°	0.01	13	69°	2.60	1,0
	0.02	25.5	69°	2.60	1,02
	0.03	35.5	64°	2	0.85
	0.04	36	7°	0.12	0.07
	0.05	37	12°	0.21	0,14
	0.06	38	14°	0.25	0,20
	0.07	39	16°	0.29	0,26
	0.08	40.5	21°	0.38	0,38
	0,09	43	24°	0.44	0,46
	0.10	46	28°	0.53	0,58
	0.11	49	34°	0.67	0,75
	0.12	52	37°	0.75	0,87
	0.13	55	40°	0.84	0,99
	0.14	58.5	42°	0.90	1,08
	0.15	63	42°	0.90	1,07
	0.16	67.5	42°	0.90	1.07
	0.17	72.5	42°	0.90	1,06
	0.18	77.5	42°	0.90	1,05
	0.19	82	40°	0.84	0,98
	0.20	86.5	38°	0.78	0,90
	0.21	90.5	36°	0.73	0,85
	0.22	94	31°	0.60	0,70
	0.23	97	25°	0.47	0,56

TABLE N° 7 (cont.)

Temperature	ε_t	σ [kgr/mm²]	$d\sigma/d\varepsilon_t$ [α]	$d\sigma/d\varepsilon_t = tg\alpha$ [×500Kgr/mm²]	$n = \frac{\varepsilon_t}{\sigma} \times \frac{d\sigma}{d\varepsilon}$
0°	0.01	15	70°	2.75	0.92
	0.02	29	70°	2.75	0.95
	0.03	42	69°	2.60	0.93
	0.04	51	50°	1.19	0.47
	0.05	52,5	12°	0.21	0.10
	0.06	53,5	12°	0.21	0.12
	0.07	54,5	18°	0.32	0.21
	0.08	56	27°	0.51	0.37
	0.09	58,5	30°	0.58	0.45
	0.10	61	30°	0.58	0.48
	0.11	64	30°	0.58	0.50
	0.12	67,3	30°	0.58	0.52
	0.13	70,5	30°	0.58	0.54
	0.14	73,5	30°	0.58	0.55
	0.15	76,5	30°	0.58	0.57
	0.16	79,5	30°	0.58	0.59
	0.17	83	30°	0.58	0.60
	0.18	86	30°	0.58	0.61
	0.19	89	29,5°	0.57	0.61
	0.20	91,5	29°	0.55	0.60
	0.21	95	28°	0.53	0.59
-54°	0.01	15	70°	2.75	0.92
	0.02	30	70°	2.75	0.92
	0.03	45	70°	2.75	0.92
	0.04	59,5	70°	2.75	0.93
	0.05	69,5	61°	1.80	0.65
	0.06	72	32°	0.62	0.26
	0.07	73,5	19°	0.34	0.16
	0.08	74	8°	0.14	0.08
	0,09	74,5	6°	0.10	0.06
	0.10	75,5	11°	0.19	0.13
	0.11	76,5	14°	0.25	0.18
	0.12	77,5	16°	0.29	0.23
	0.13	79	19°	0.34	0.28
	0.14	81	21°	0.38	0.33
	0.15	83	27°	0.51	0.46
-101°	0.01	15,5	72°	3.08	0.99
	0.02	31,5	74°	3.49	1.11
	0.03	48,5	74°	3.49	1.08
	0.04	66	74°	3.49	1.06
	0.05	77	50°	1.19	0.39
	0.06	80,5	28°	0.53	0.20
-193°	0.01	15,5	73°	3.27	1.06
	0.02	31	73°	3.27	1.06
	0.03	47	73,5°	3.37	1.08
	0.04	64	74°	3.49	1.09
	0.05	82	75°	3.73	1.14
	0.06	98,5	75°	3.73	1.14

Figure captions

Fig.1 Schematic representation of a stress-strain curve showing the pseudoelastic behaviour [74KRI].

Fig.2 Schematic representation of the interrelationships between stress-assisted (below M_s^σ) and strain-induced (above M_s^σ) martensitic transformation [72OLS].

Fig.3 Orientation relationships between (ß) body-centred cubic matrix and (α') hexagonal close packed martensite [34BUR].

Fig.4 Transition of the body-centred cubic into the hexagonal close packed lattice in zirconium [34BUR]. S represents a shear on a $(1\bar{1}2)$ plane along a $[\bar{1}11]$ direction.

Fig.5 Phases present after quenching from ß-region, as a function of Nb content. Zr-Nb and Zr-Nb-1%Al alloys.

Fig.6 M_S-Martensite start temperature as a function of Nb content.

Fig.7 Proposed stability diagram for predicting mode of deformation in zirconium alloys [72REZ]. tw = twinning; ⊥ slipping.

Fig.8 a) Tension test sample.
b) Schematical representation of B, M and K zones.
c) Transverse section of tension test sample.

Fig.9 Load - elongation experimental curves.
a) T = 100°C
b) T = 50°C
c) T = 0°C
d) T = -54°C
e) T = -101°C
f) T = -193°C

Fig. 10 Critical yield stress, as a function of temperature (tension test).

Fig.11 Ultimate tensile stress σ_{UTS} and plastic deformation as a function of temperature.

Fig. 12 Optical microscopy on B (Bruch), M (Medium) and K (Kopf) zones.

a) From sample tested at T = 100°C
b) " " " " T = 50°C
c) " " " " T = 0°C
d) " " " " T = -54°C
e) " " " " T = -101°C
f) " " " " T = -193°C

Fig. 13 Scanning electron Microscopy

Fig. 14 Hardening coefficient $\underline{n}$ versus true plastic deformation ε_t, for the six tension tests.

Fig. 15 True stress versus true plastic deformation, for the six tension tests.

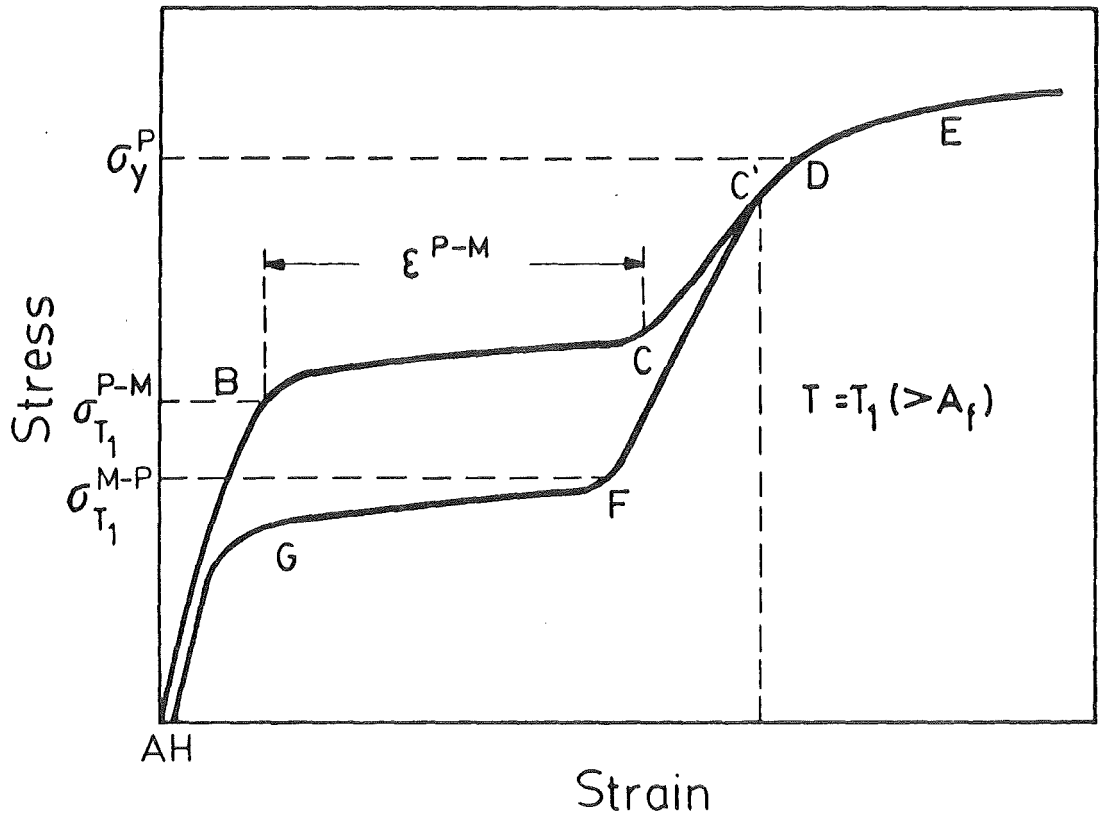

Fig.1 Schematic representation of a stress-strain curve showing the pseudoelastic behaviour [74KRI].

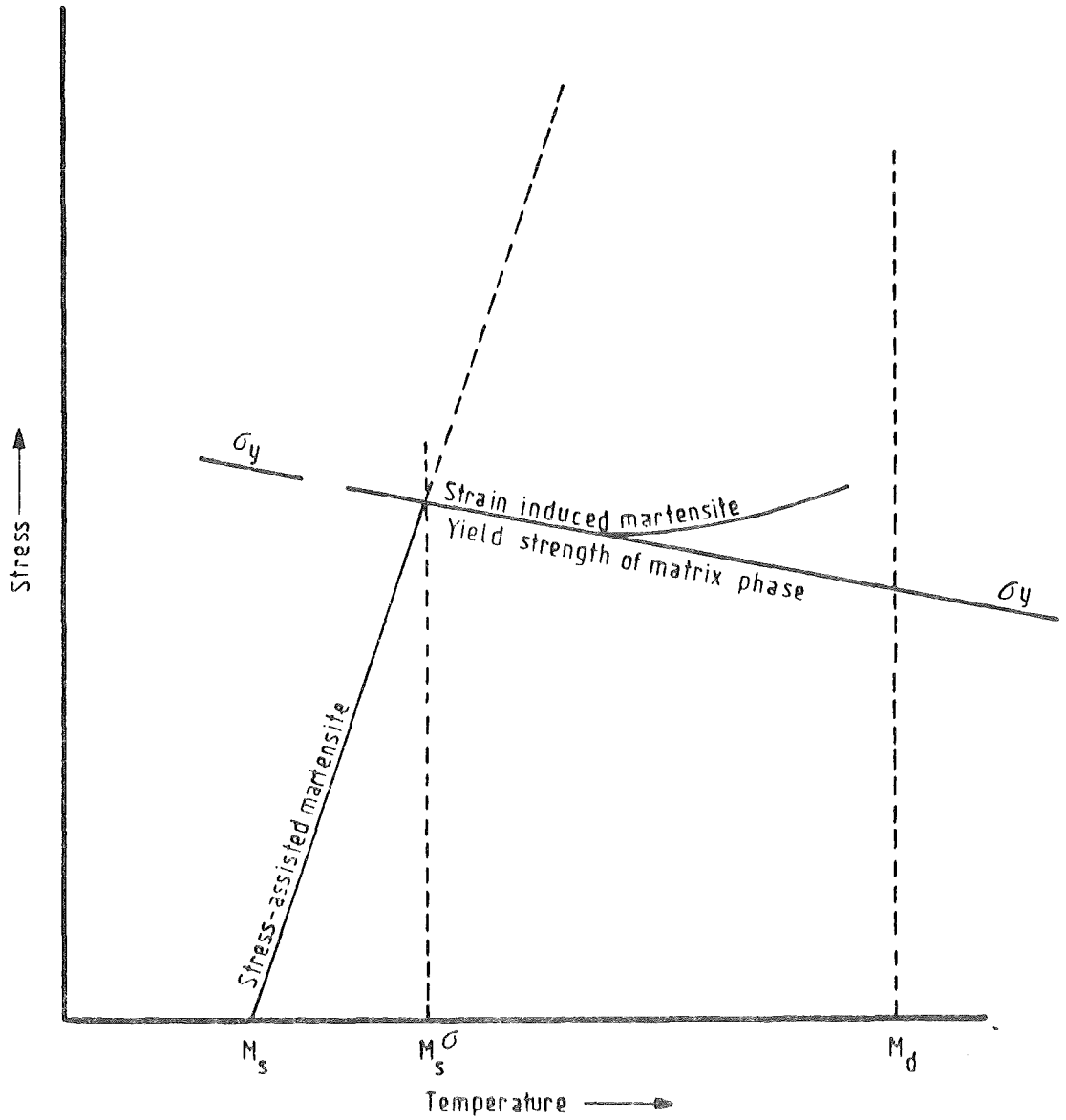

Fig.2 Schematic representation of the interrelationships between stress-assisted (below M_s^σ) and strain-induced (above M_s^σ) martensitic transformation [720LS].

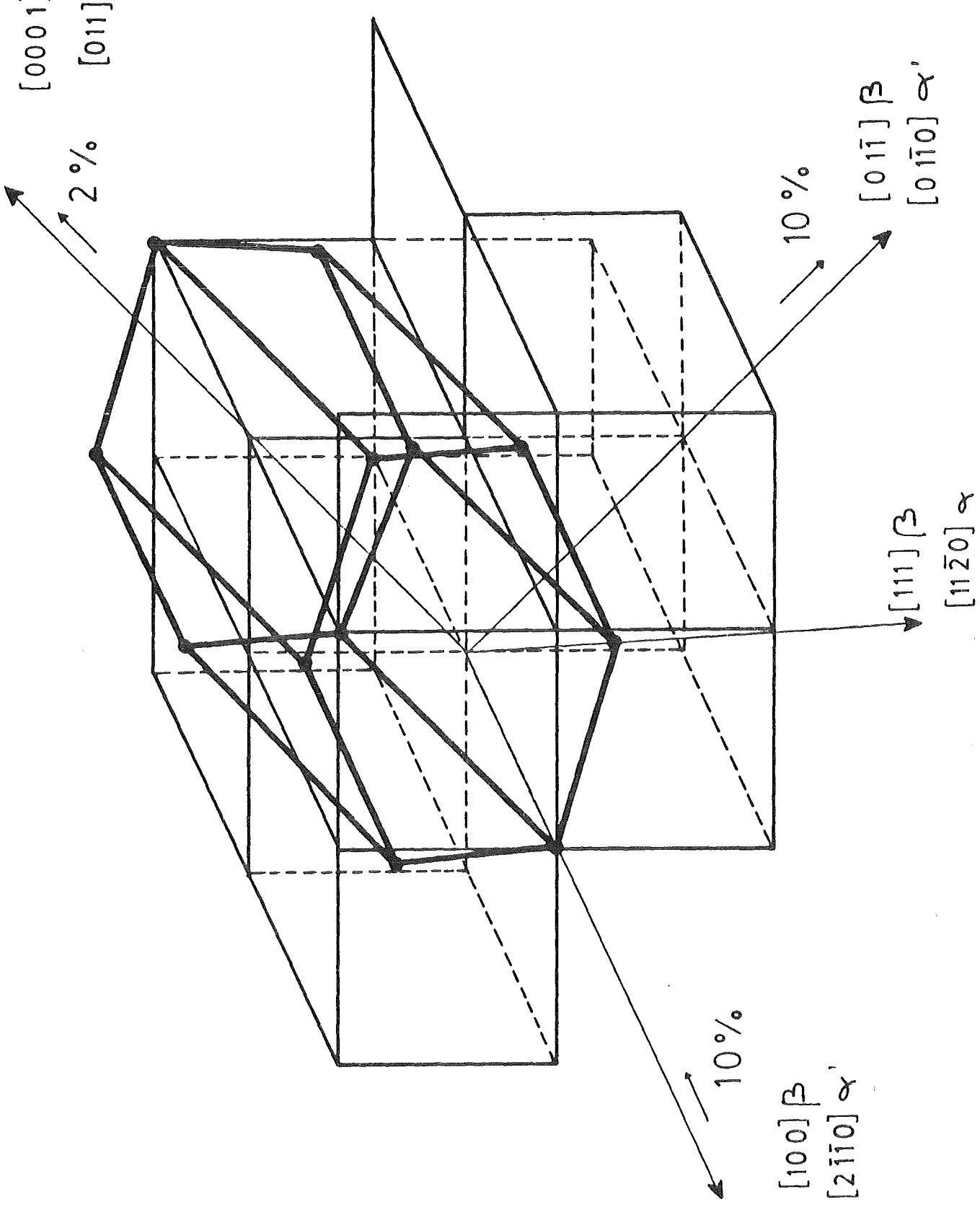

Fig.3 Orientation relationships between (ß) body-centred cubic matrix and (α') hexagonal close packed martensite [34BUR].

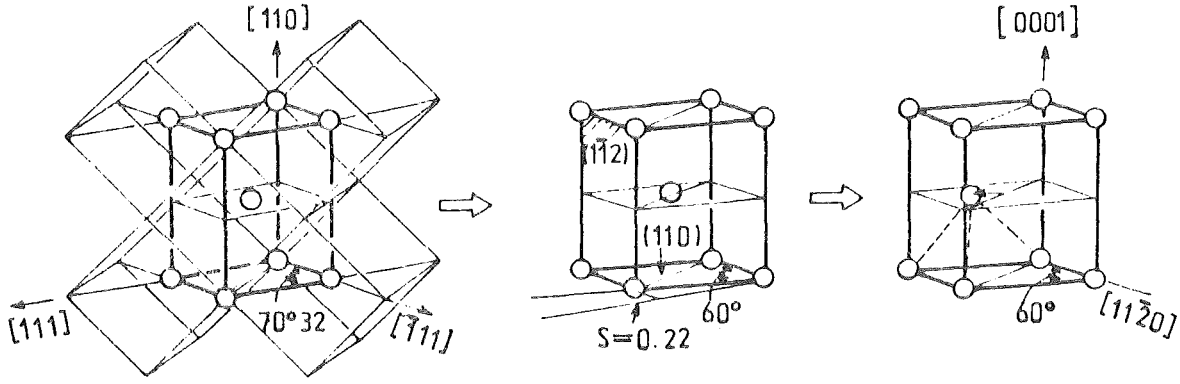

Fig.4 Transition of the body-centred cubic into the hexagonal close packed lattice in zirconium [34BUR]. S represents a shear on a $(1\bar{1}2)$ plane along a $[\bar{1}11]$ direction.

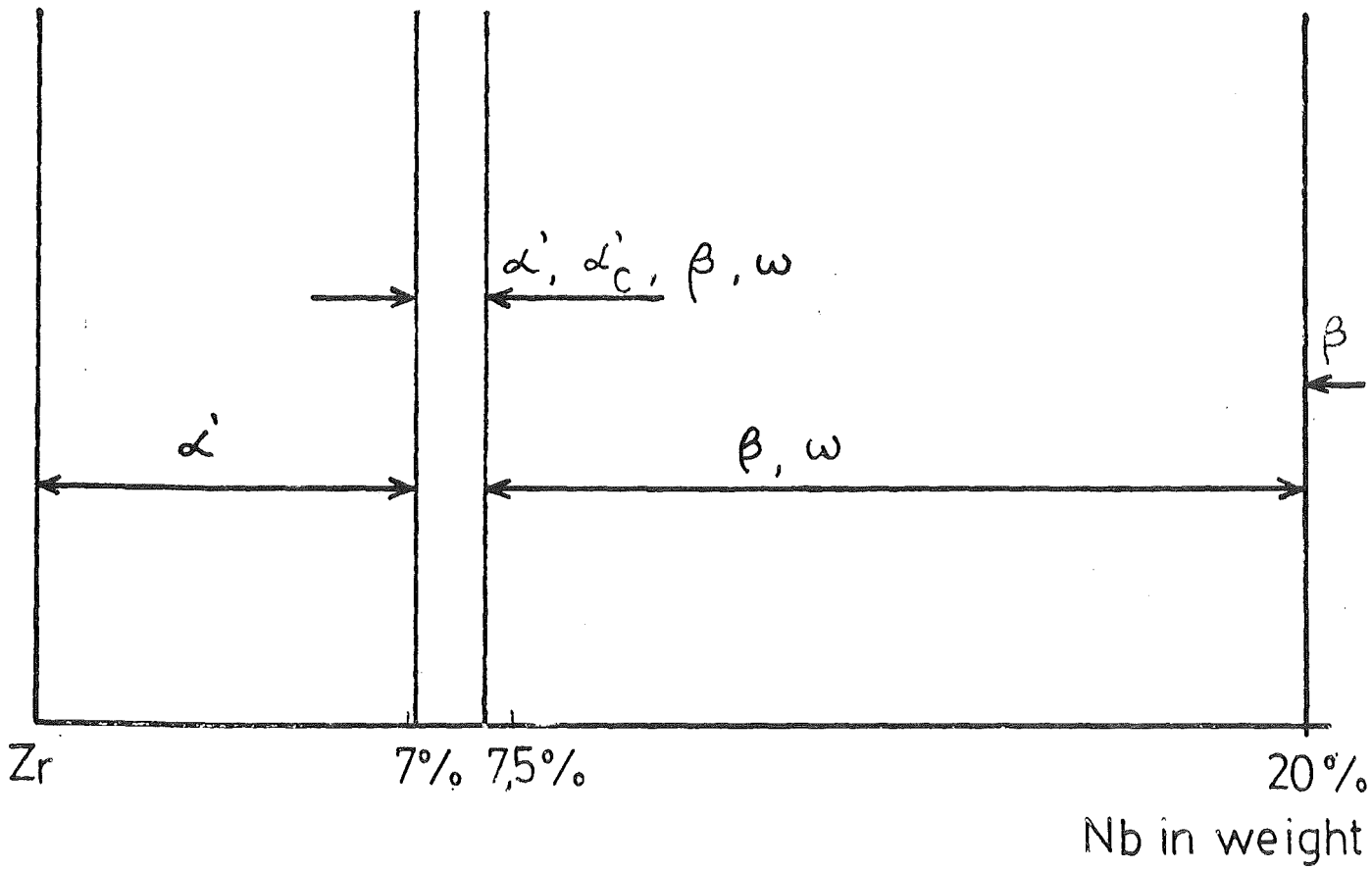

Fig.5 Phases present after quenching from ß-region, as a function of Nb content. Zr-Nb and Zr-Nb-1%Al alloys.

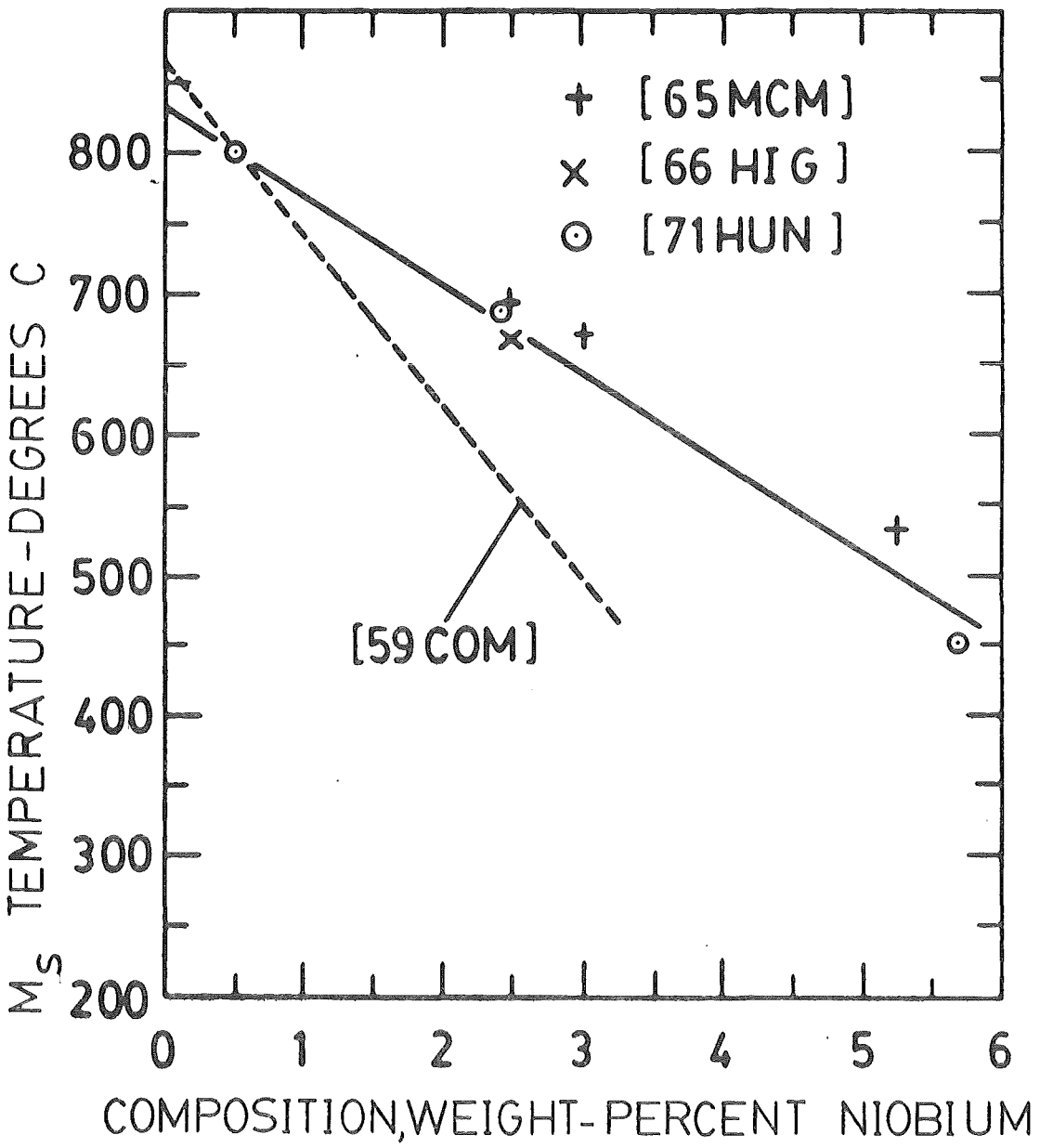

Fig.6 M_S-Martensite start temperature as a function of Nb content.

Fig.7 Proposed stability diagram for predicting mode of deformation in zirconium alloys [72REZ]. tw = twinning; ⊥ slipping.

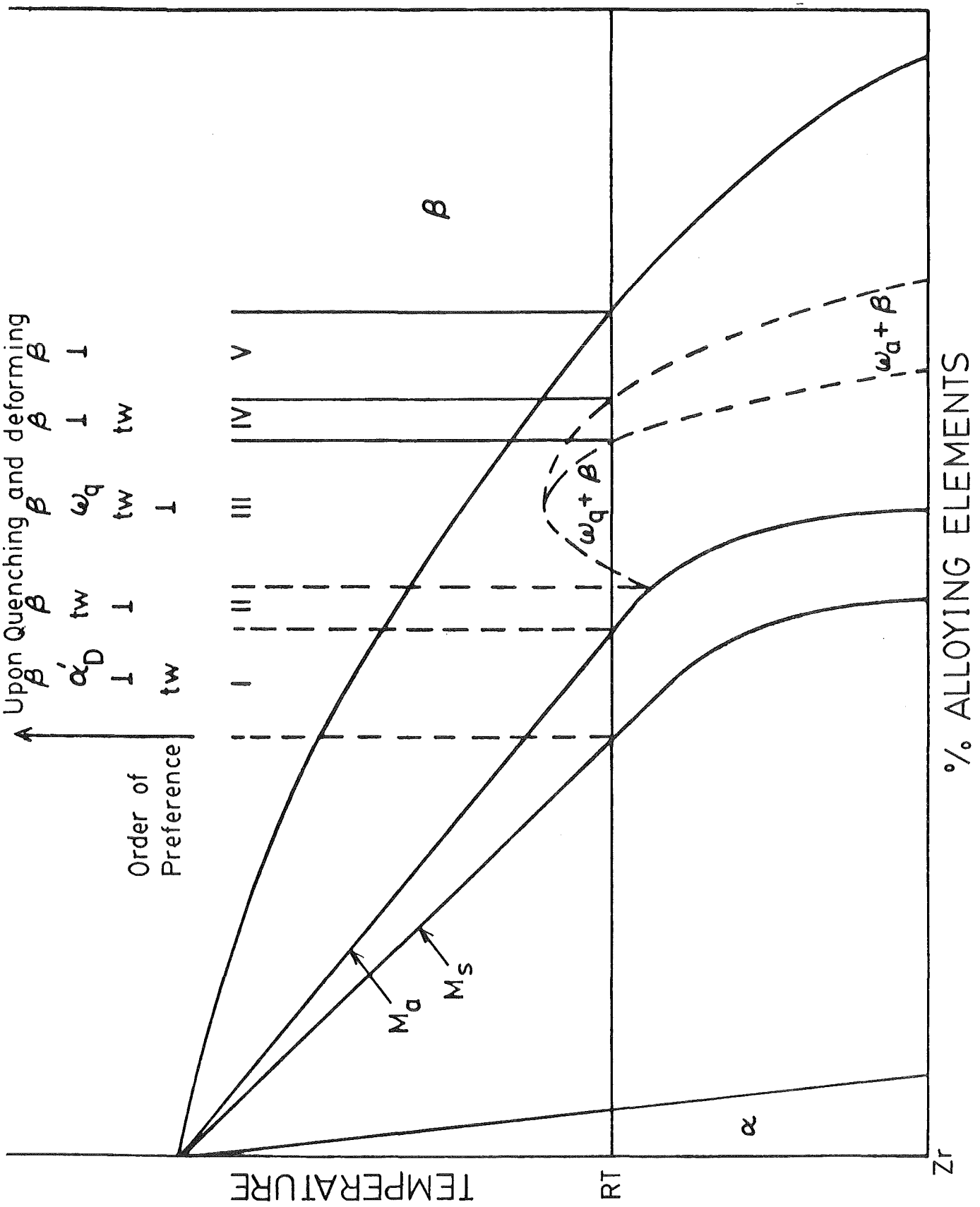

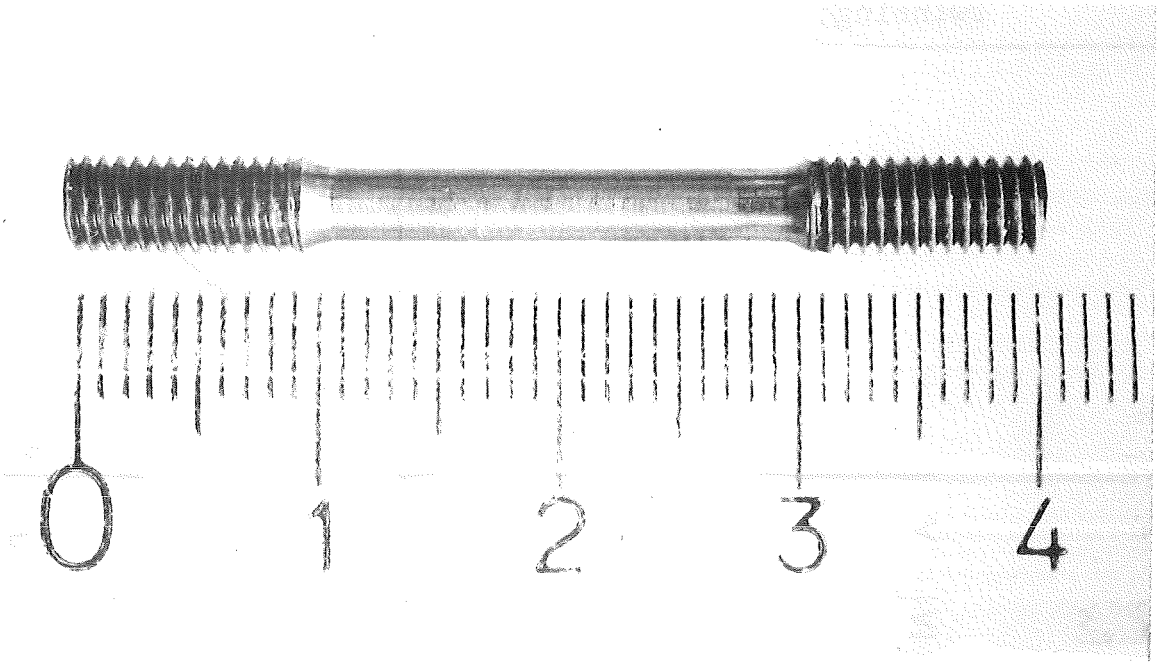

Fig.8 a) Tension test sample.

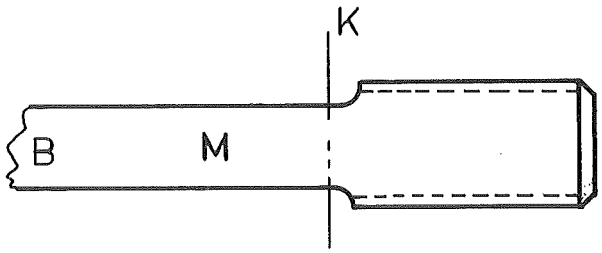

b) Schematical representation of B, M and K zones.

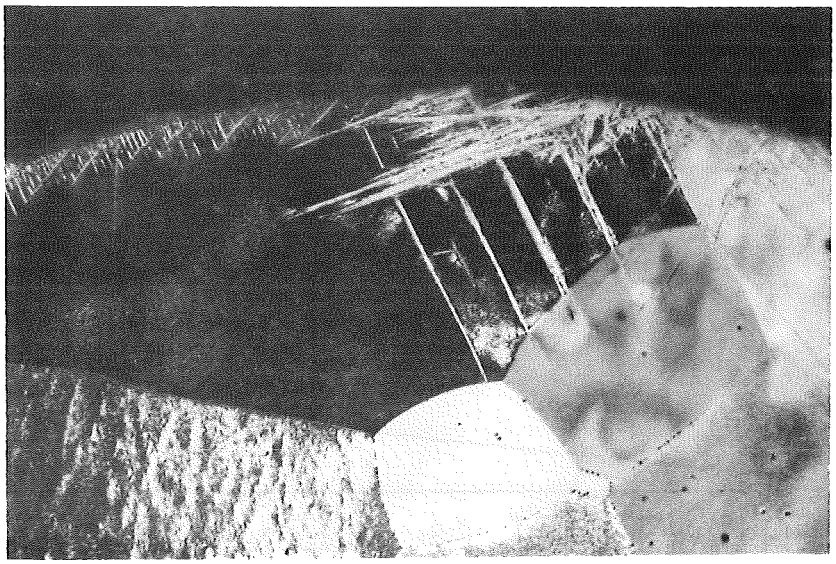

c) Transverse section of tension test sample.

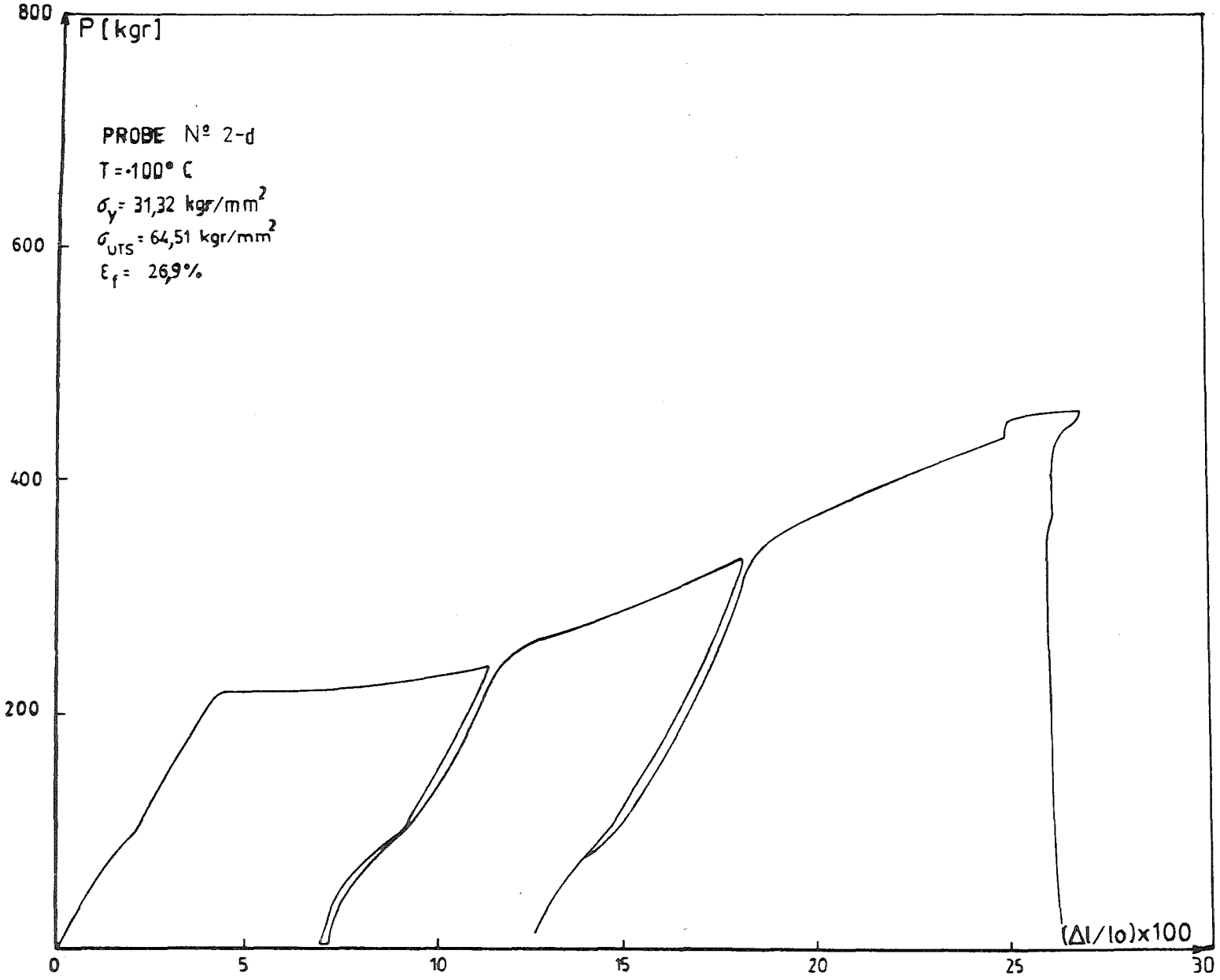

Fig. 9 a) Load - elongation experimental curve at T = 100°C

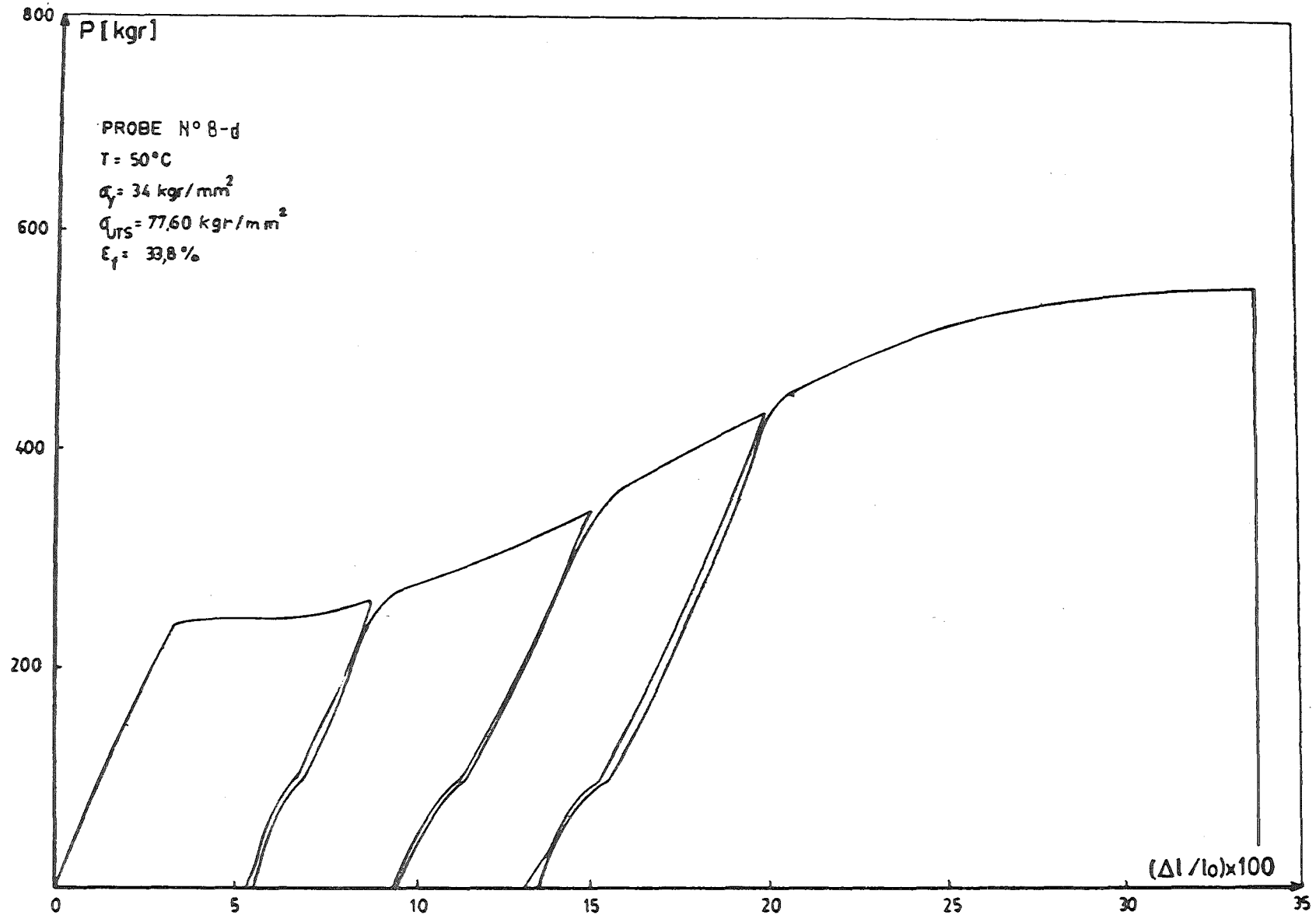

Fig. 9 b) Load - elongation experimental curve at T = 50°C

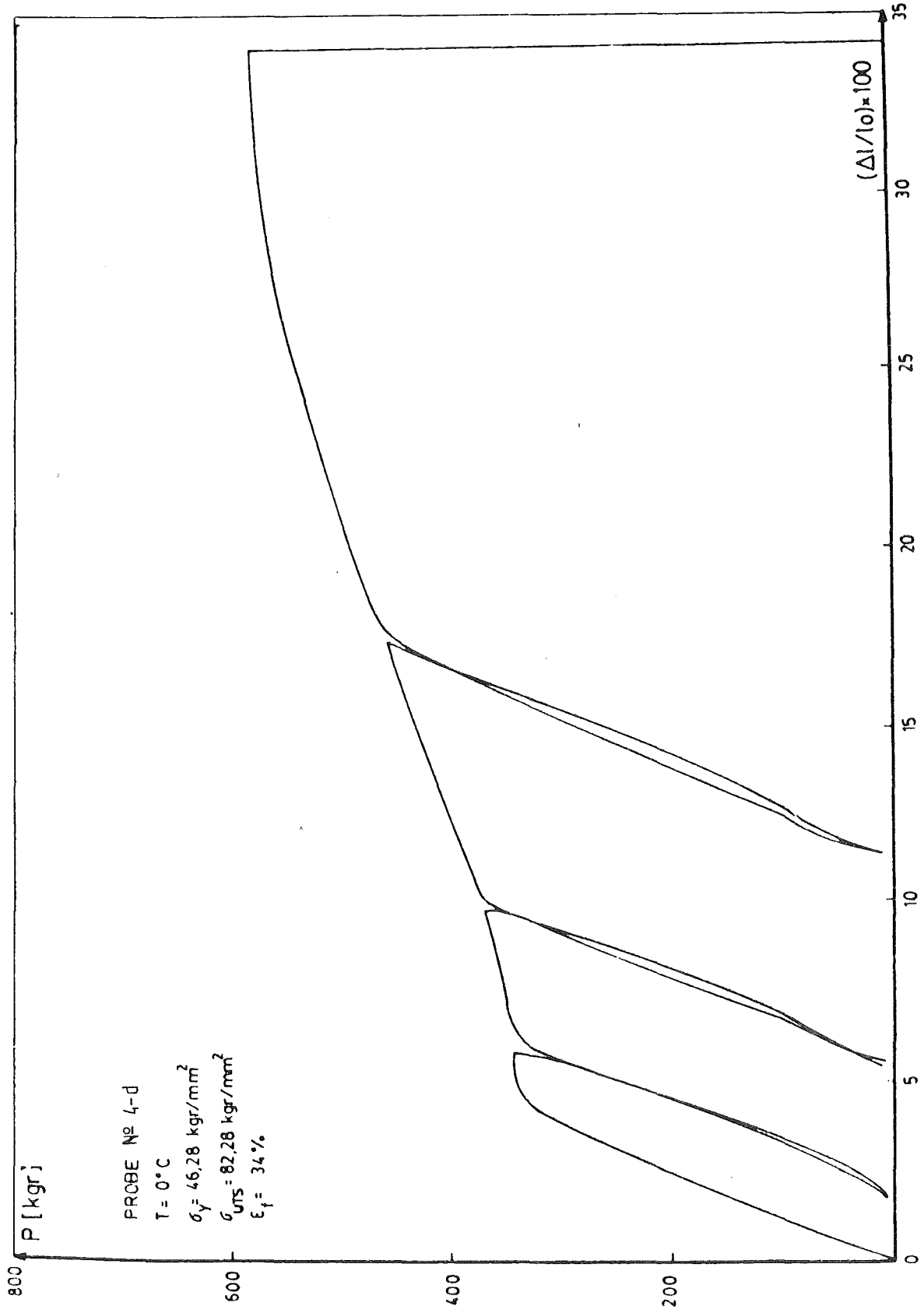

Fig. 9 c) Load - elongation experimental curve at T = 0^{o}C

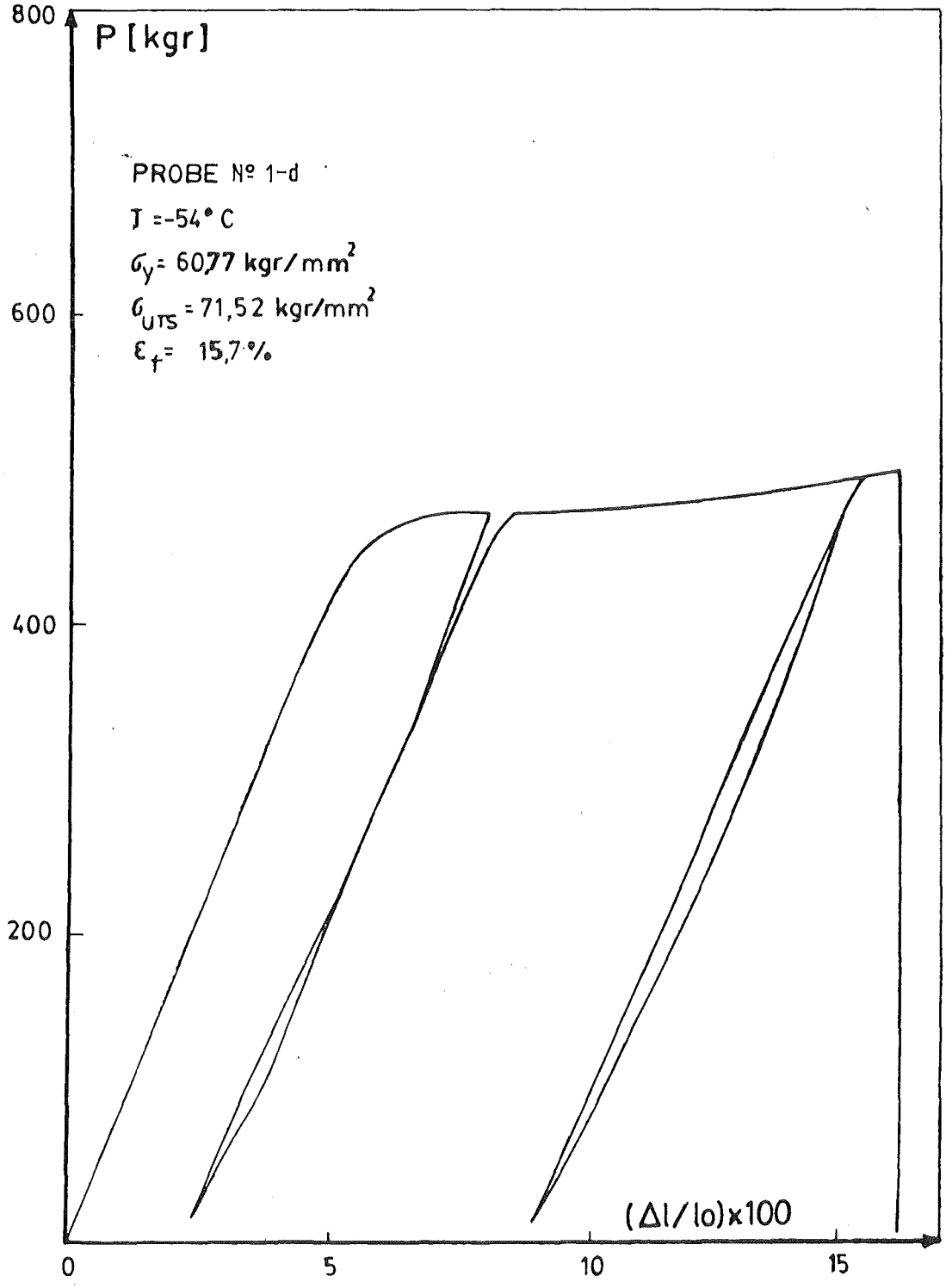

Fig. 9 d) Load - elongation experimental curve at T = -54°C

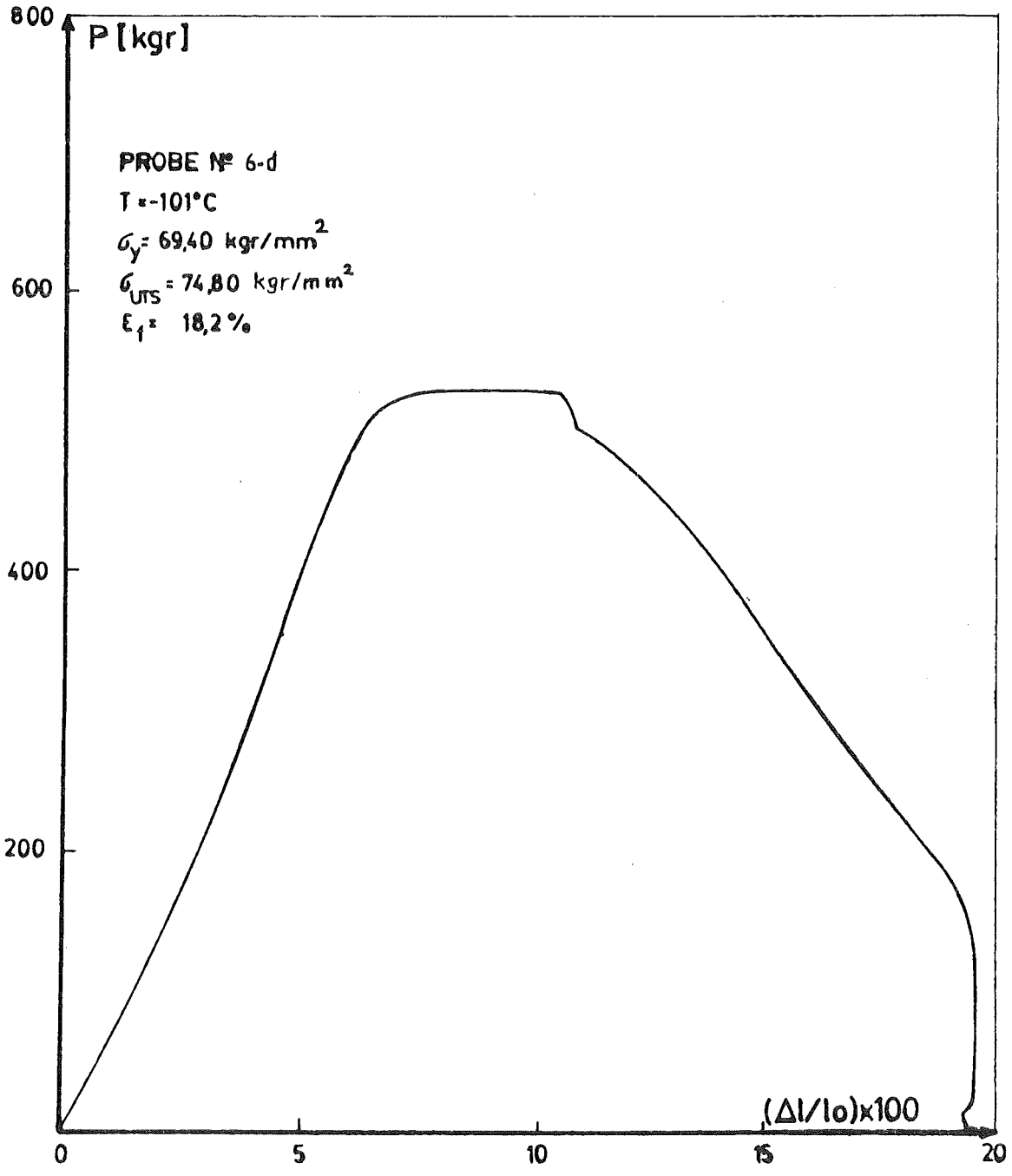

Fig. 9 e) Load - elongation experimental curve at T =-101°C

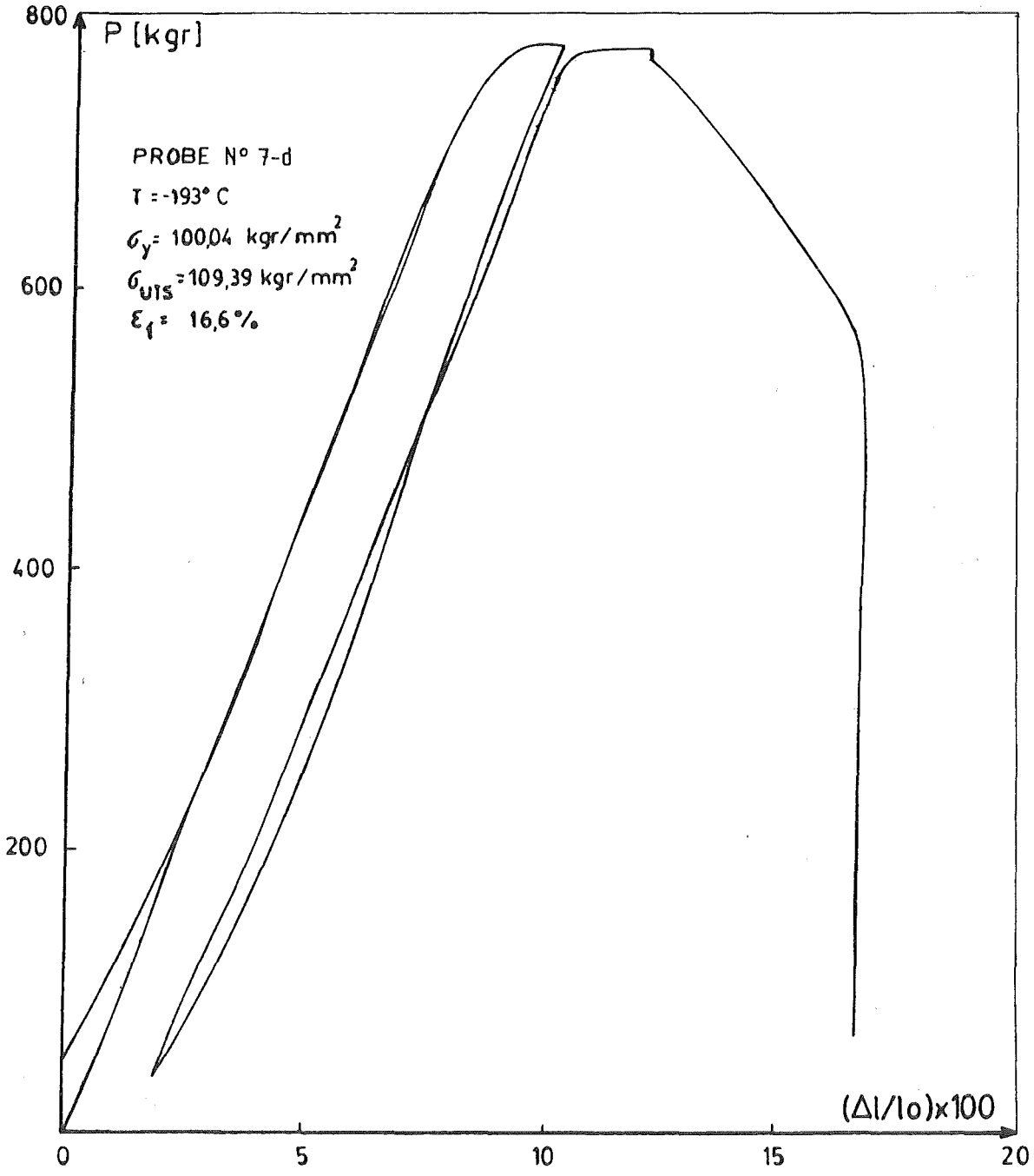

Fig. 9 f) Load - elongation experimental curve at T = -193°C

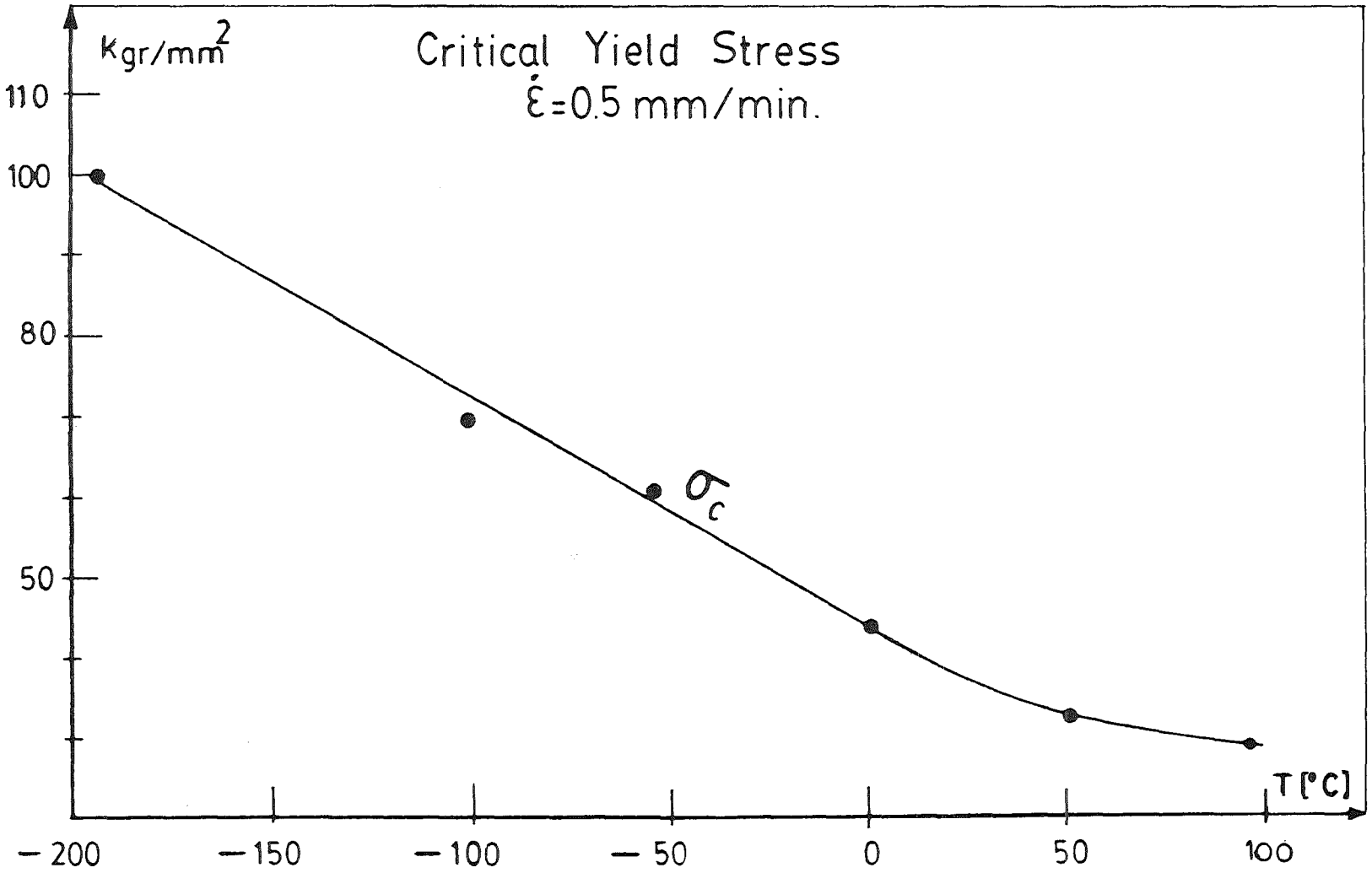

Fig. 10 Critical yield stress, as a function of temperature (tension test).

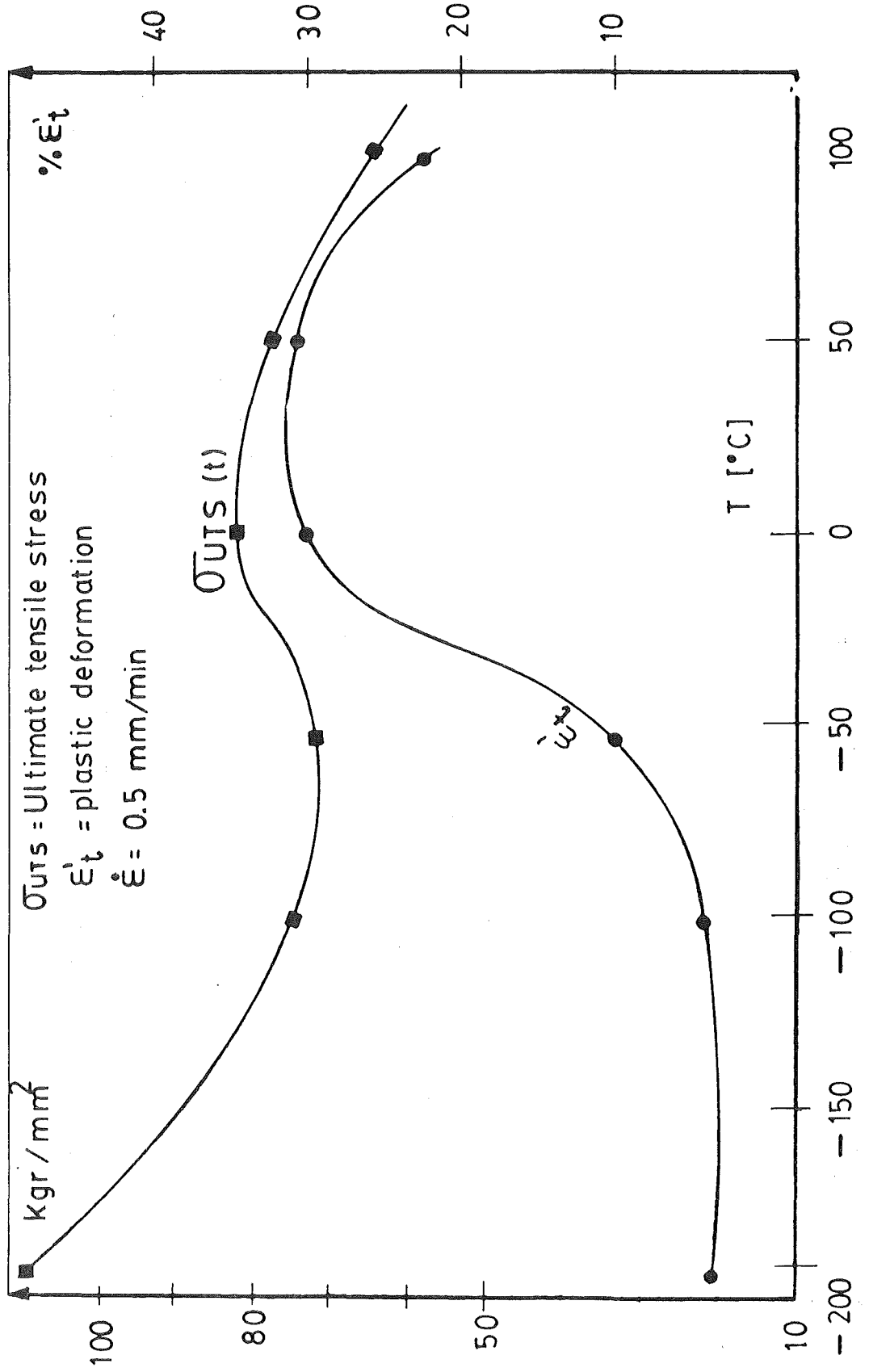

Fig.11 Ultimate tensile stress σ_{UTS} and plastic deformation as a function of temperature.

Fig. 12 Optical microscopy on B (Bruch), M (Medium) and K (Kopf) zones.

(a) From sample tested at T = 100°C
(b) " " " " T = 50°C
(c) " " " " T = 0°C
(d) " " " " T = -54°C
(e) " " " " T = -101°C
(f) " " " " T = -193°C

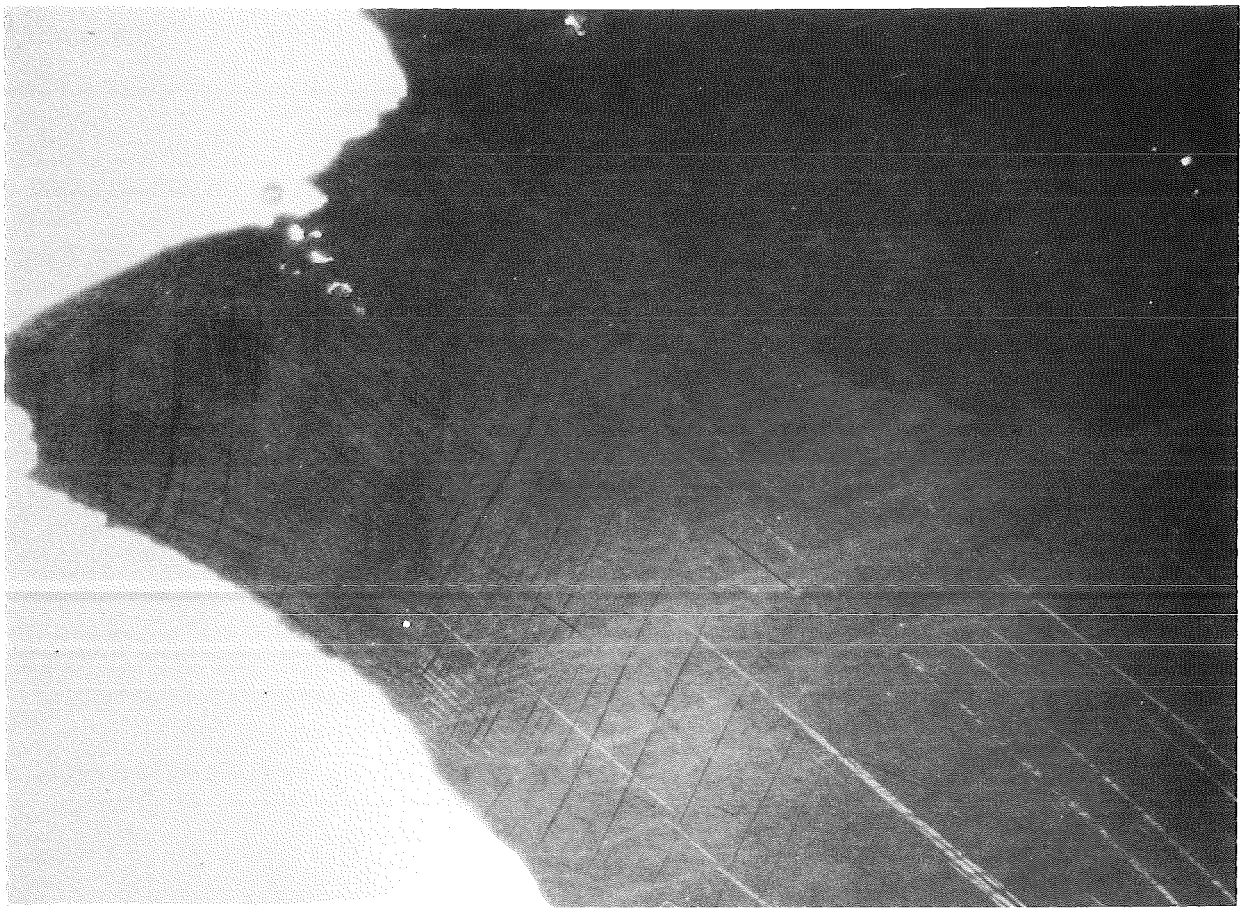

B x 100

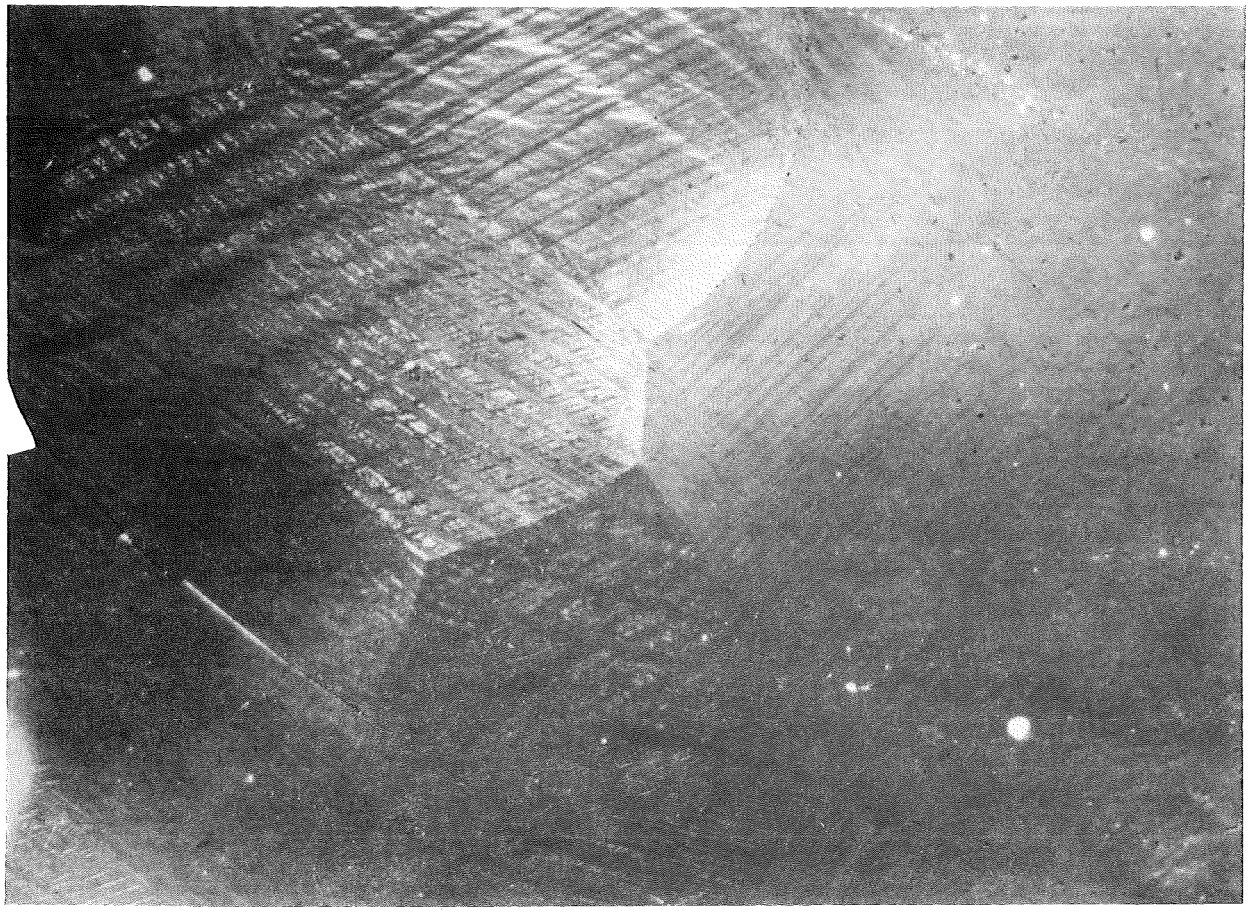

M x 100

(a) PHOTO F.O.4 PROBE 2-D T = 100°C

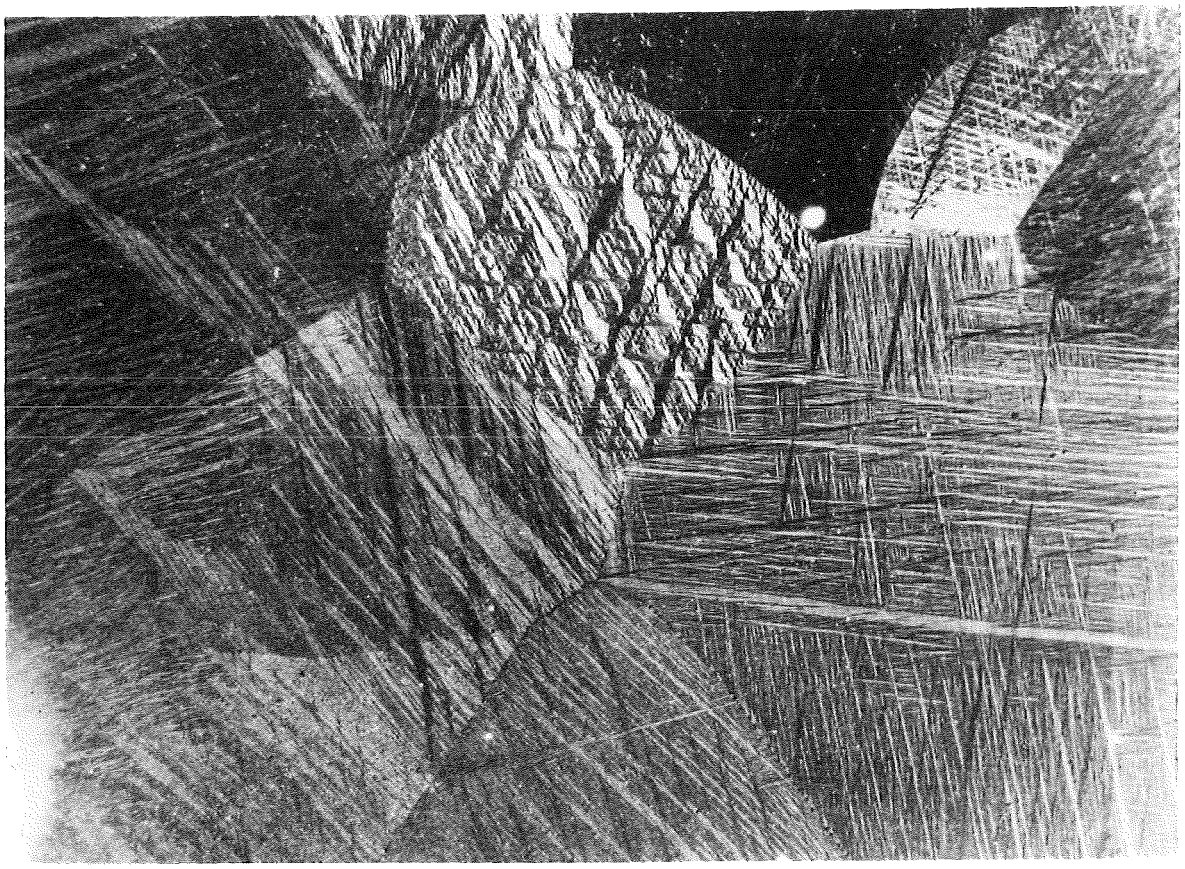

K x 100

(a) PHOTO F.O.4 PROBE 2-D T = 100°C

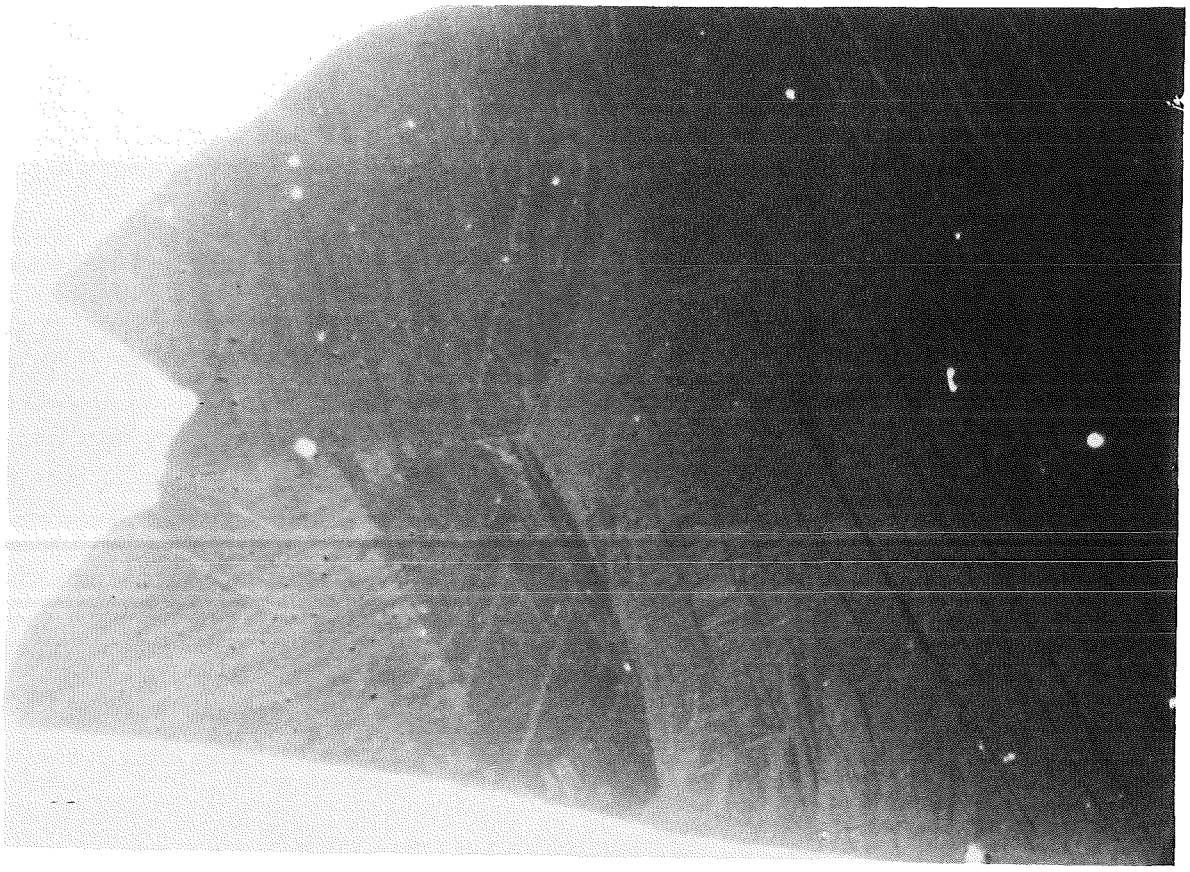

B x 100

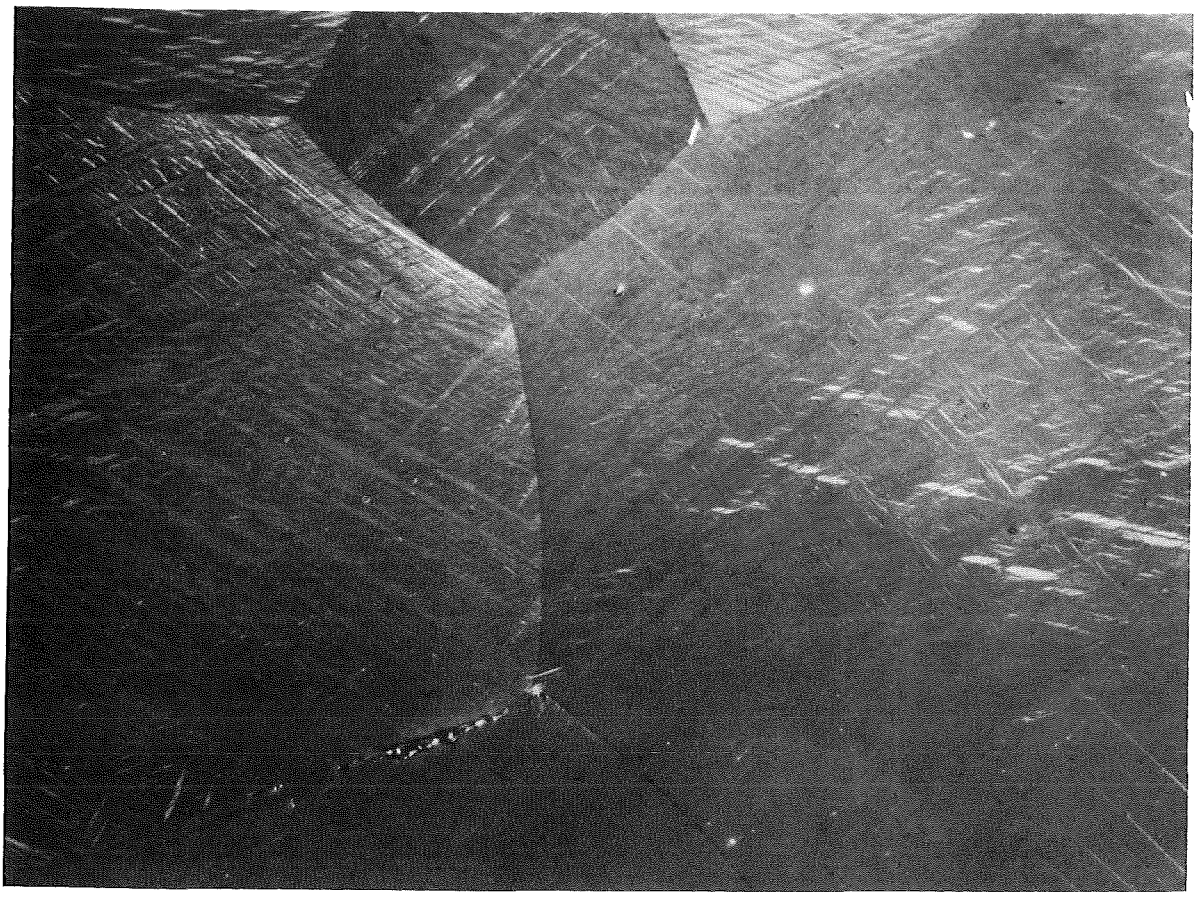

M x 100

(b) PHOTO F.O.5 PROBE 8-D T = 50°C

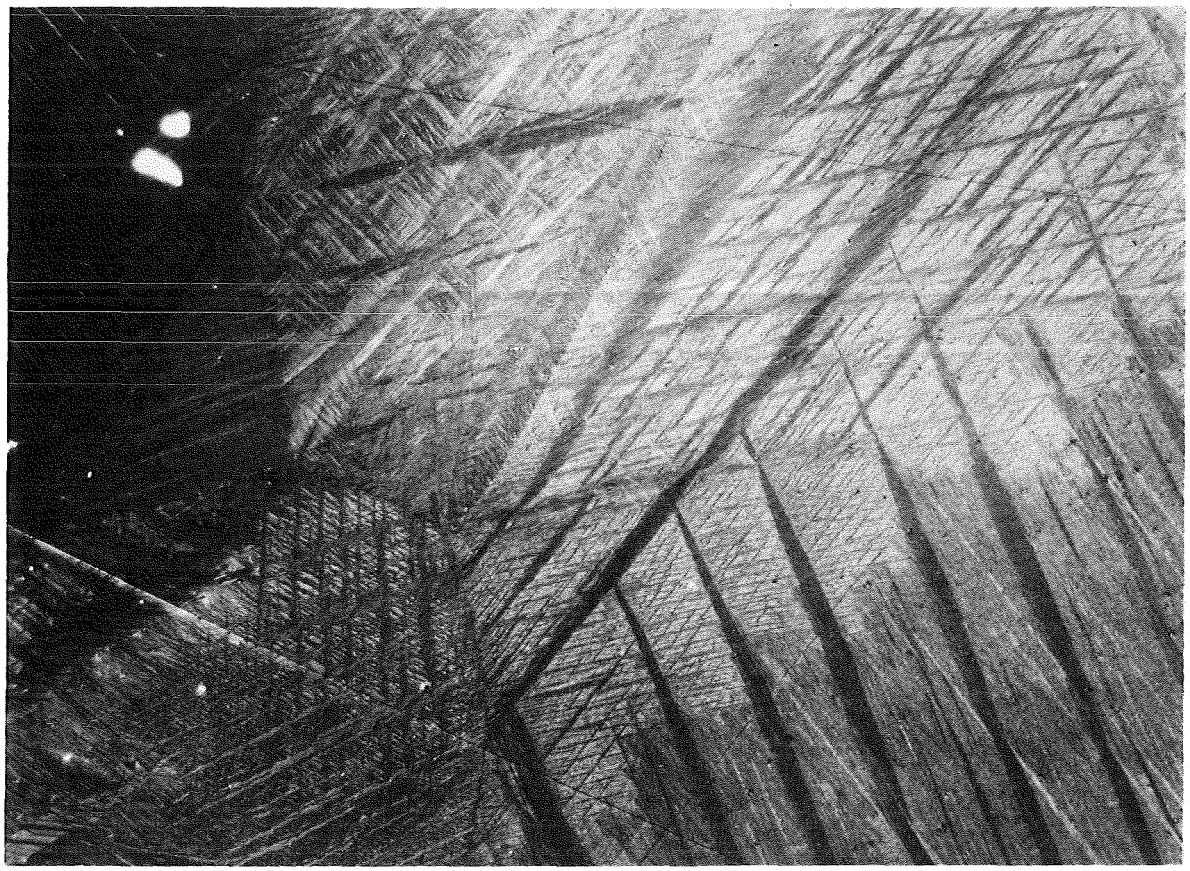

K x 100

(b) PHOTO F.0.5 PROBE 8-D T = 50°C

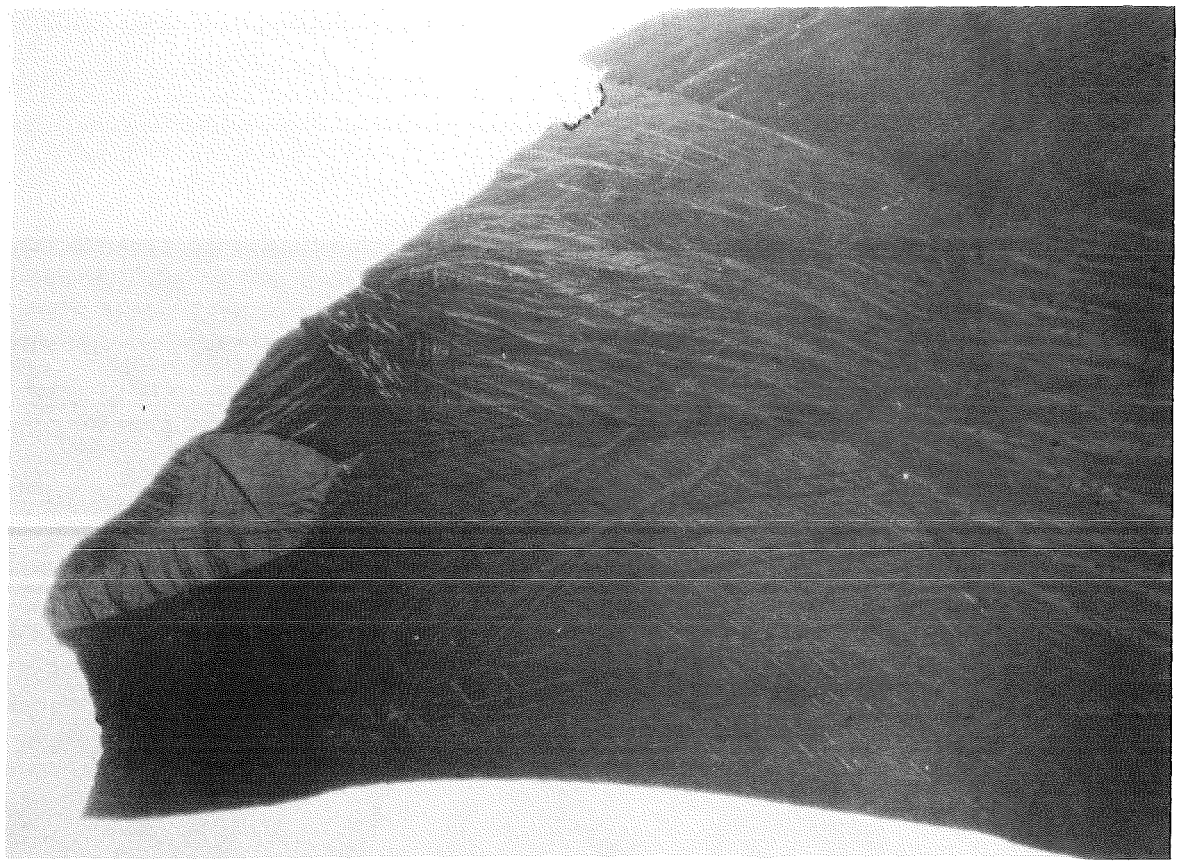

B x 100

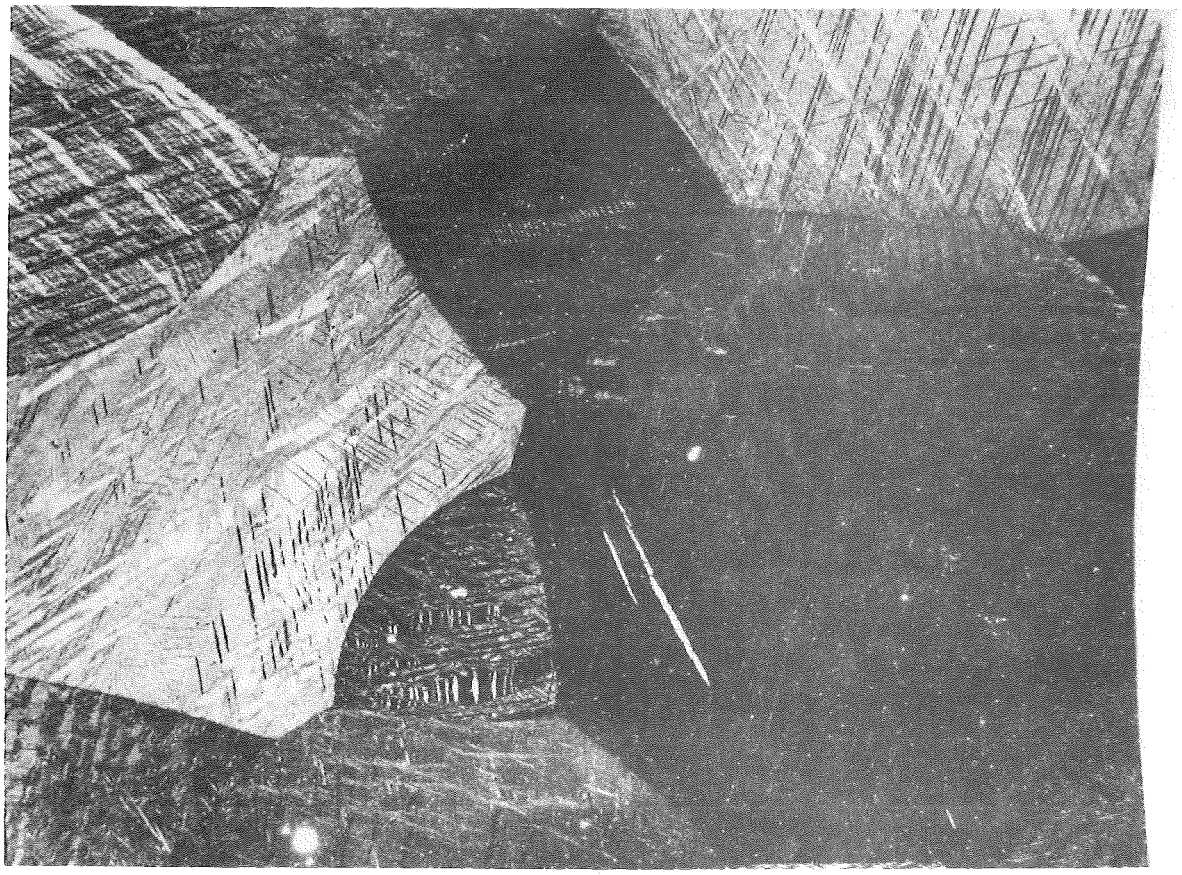

M x 100

(c) PHOTO F.O.6 PROBE 4-D T = $0^{o}C$

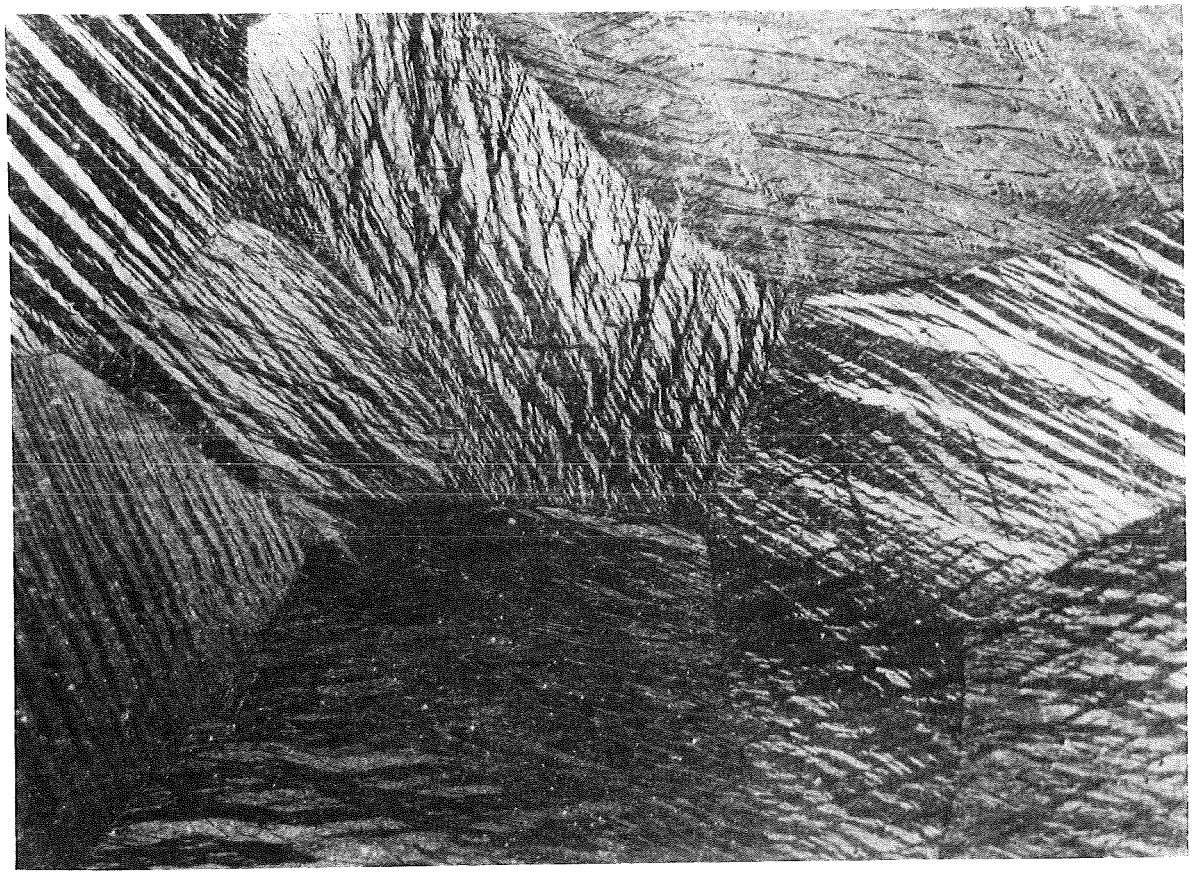

K x 100

(c) PHOTO F.O.6 PROBE 4-D T = $0^{o}C$

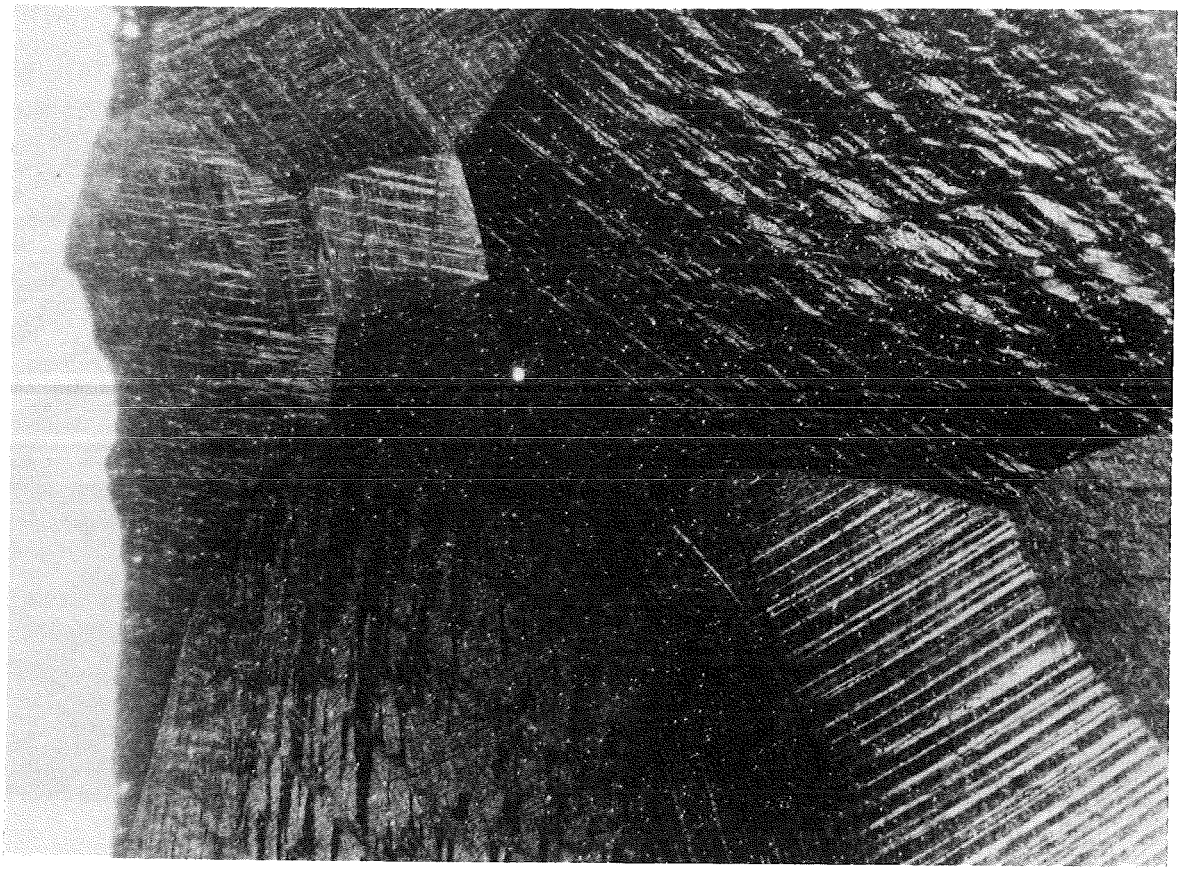

B x 100

(d) PHOTO F.O.7 PROBE 1-D T = -54°C

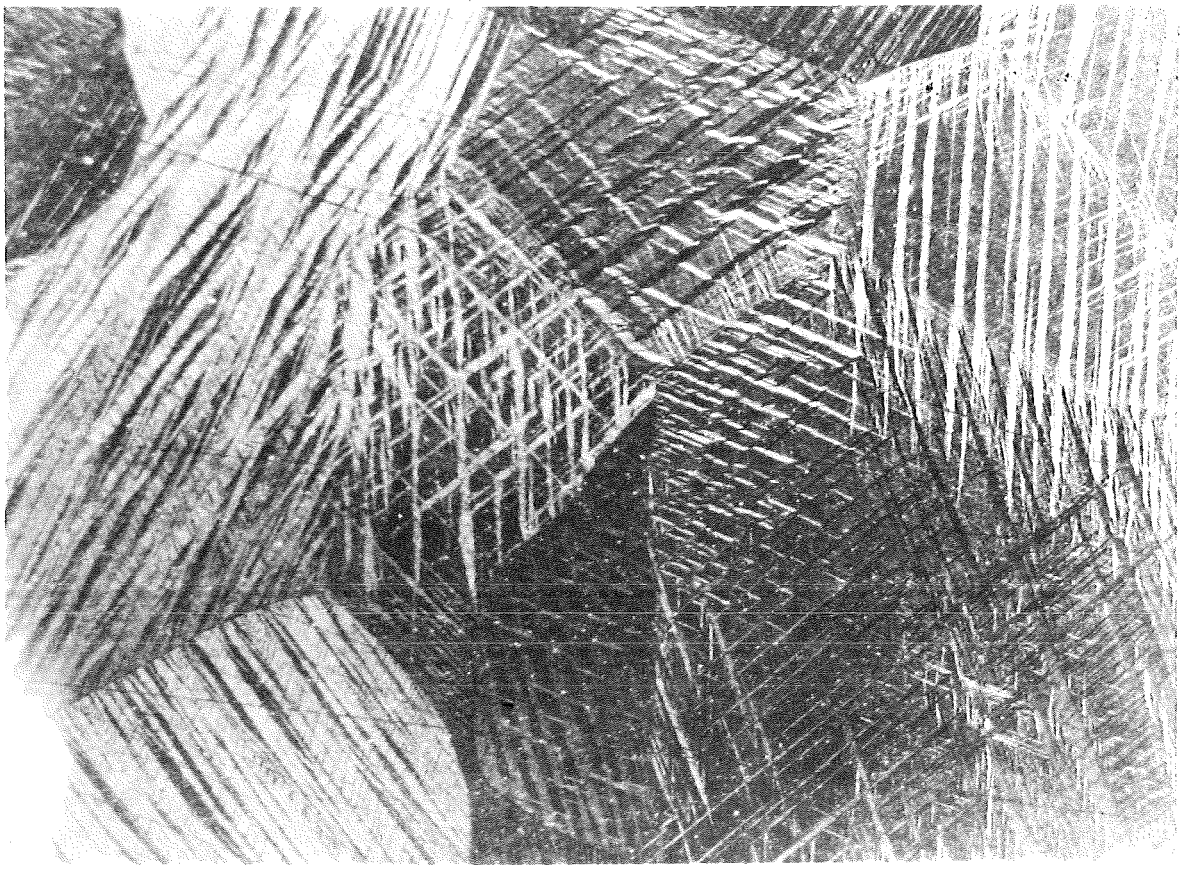

M x 100

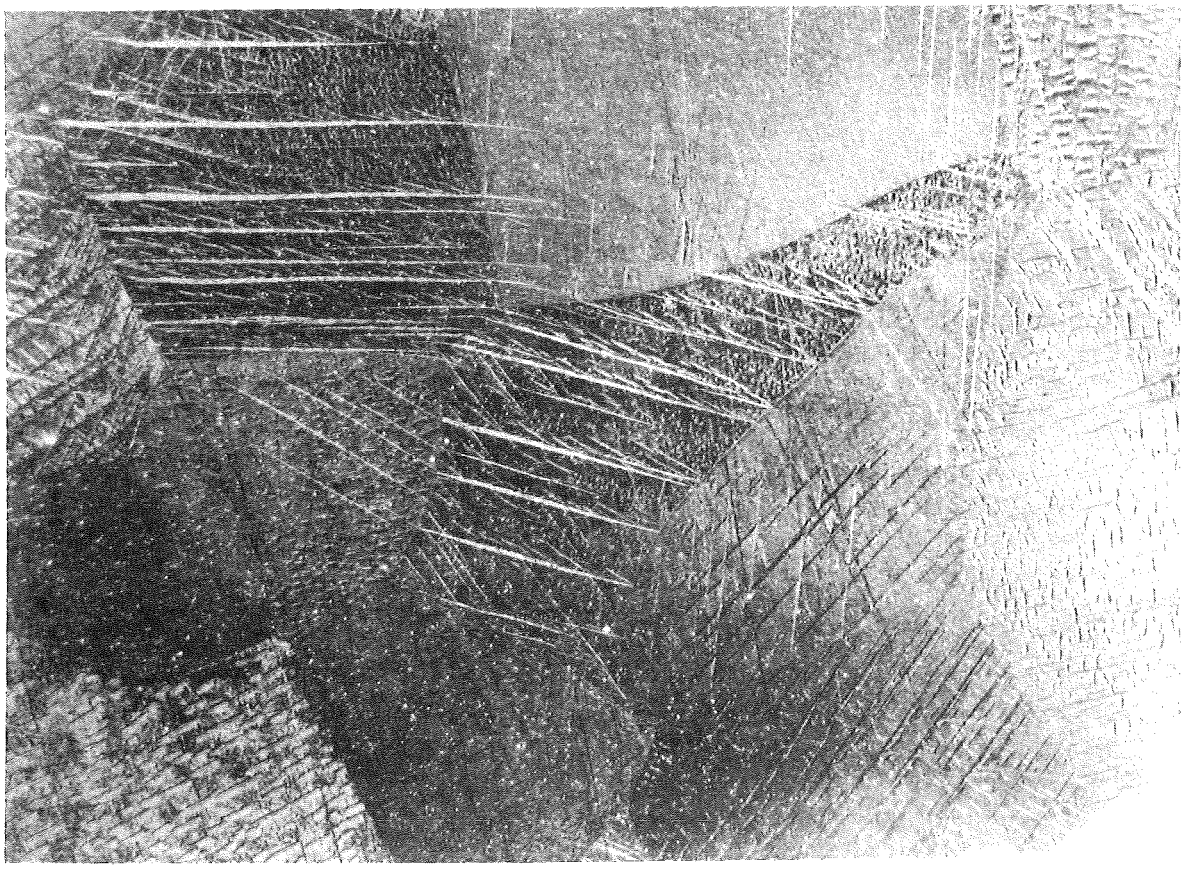

K x 100

(d) PHOTO F.O.7 PROBE 1-D T = -54°C

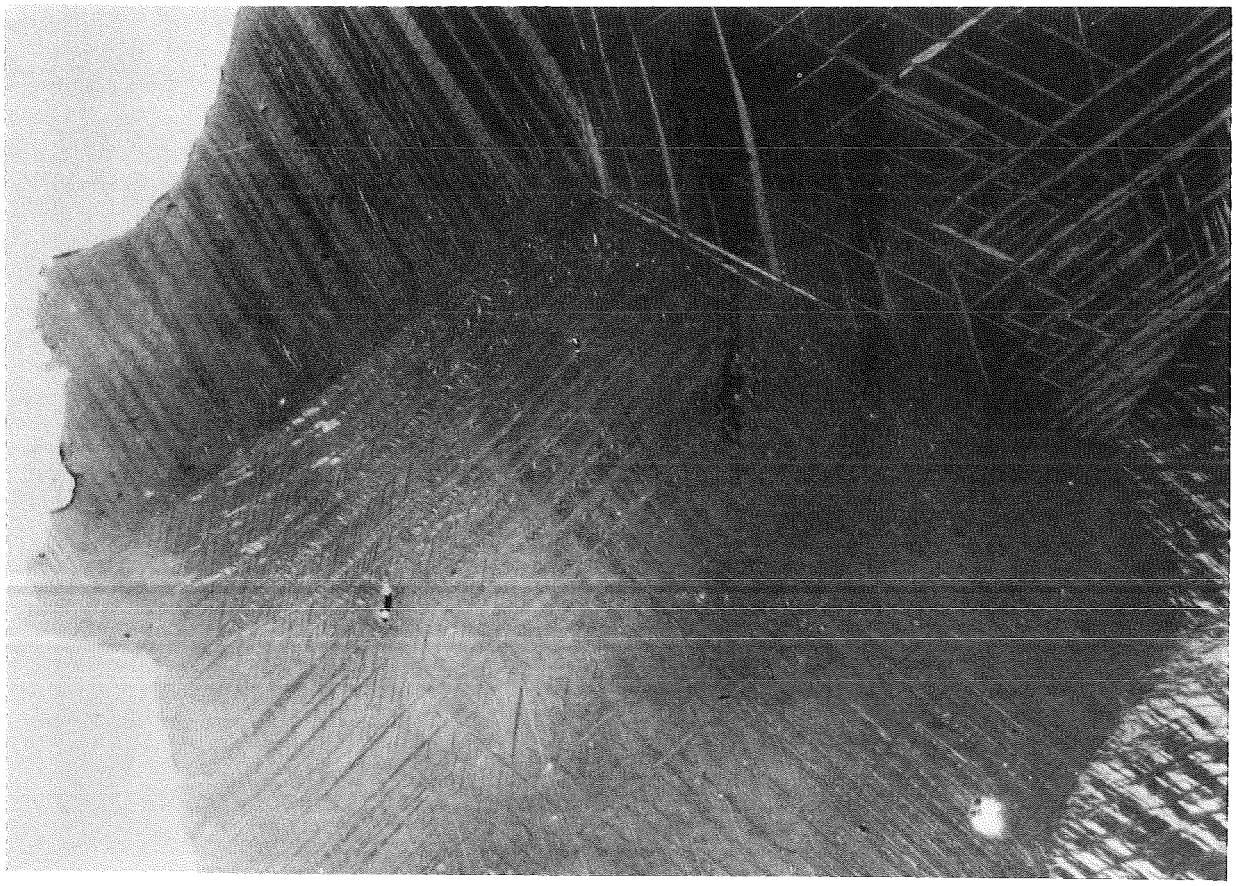

B x 100

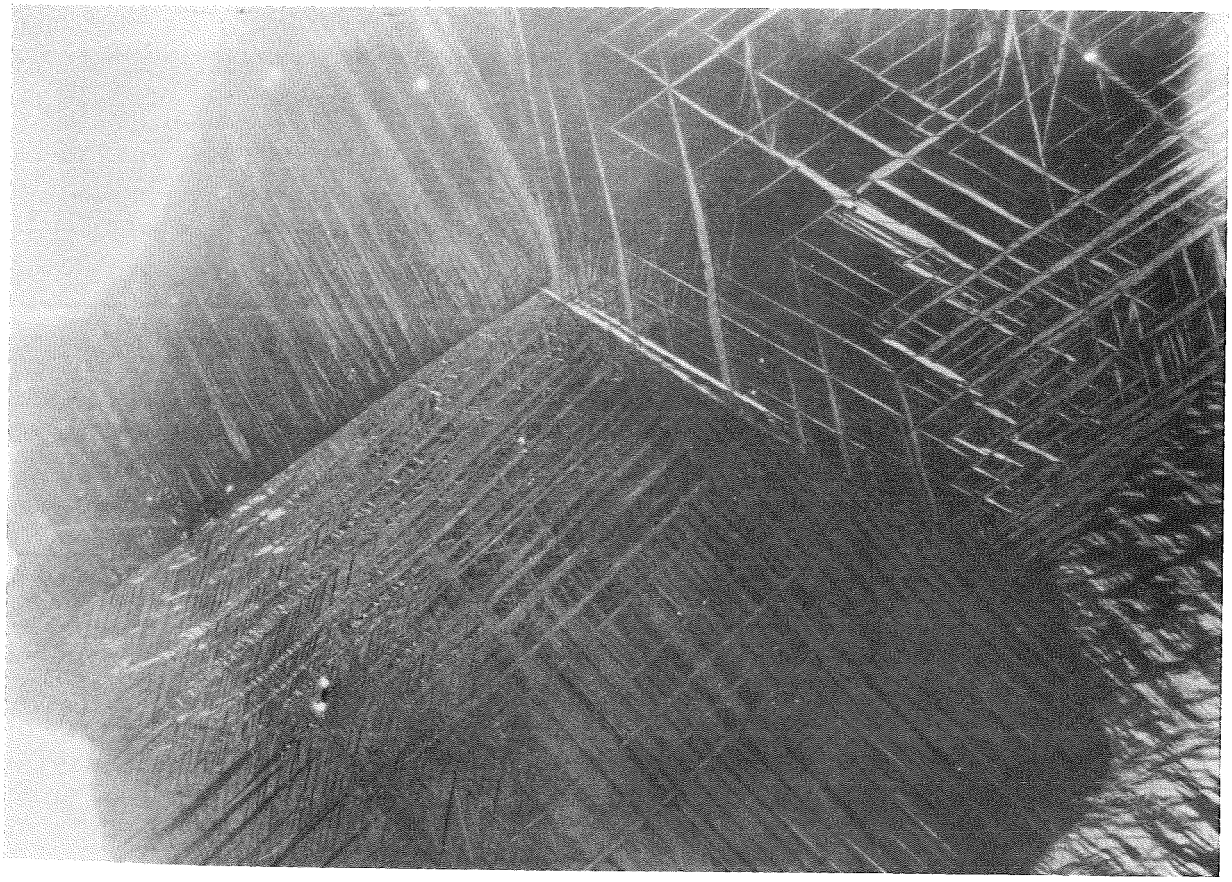

M x 100

(e) PHOTO F.O.8 PROBE 6-D T = -101°C

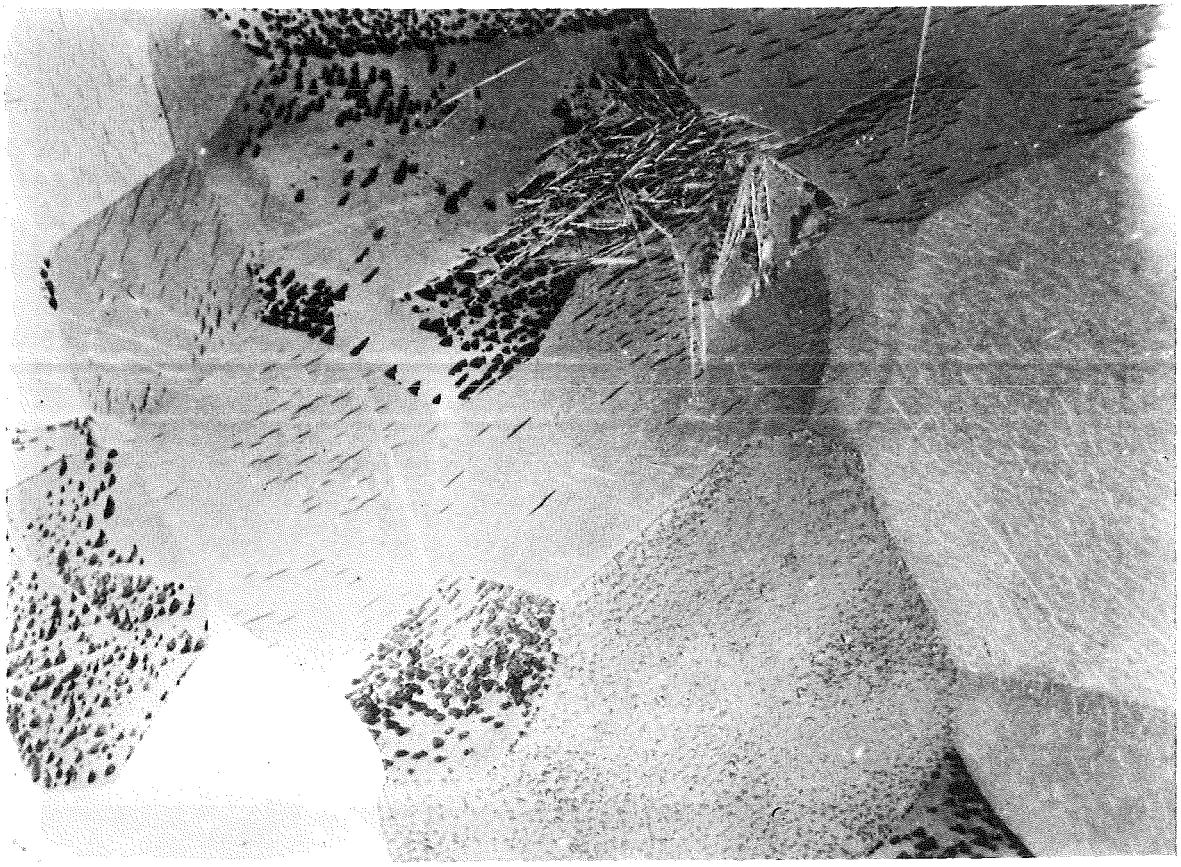

K x 100

(e) PHOTO F.O.8 PROBE 6-D T = -101°C

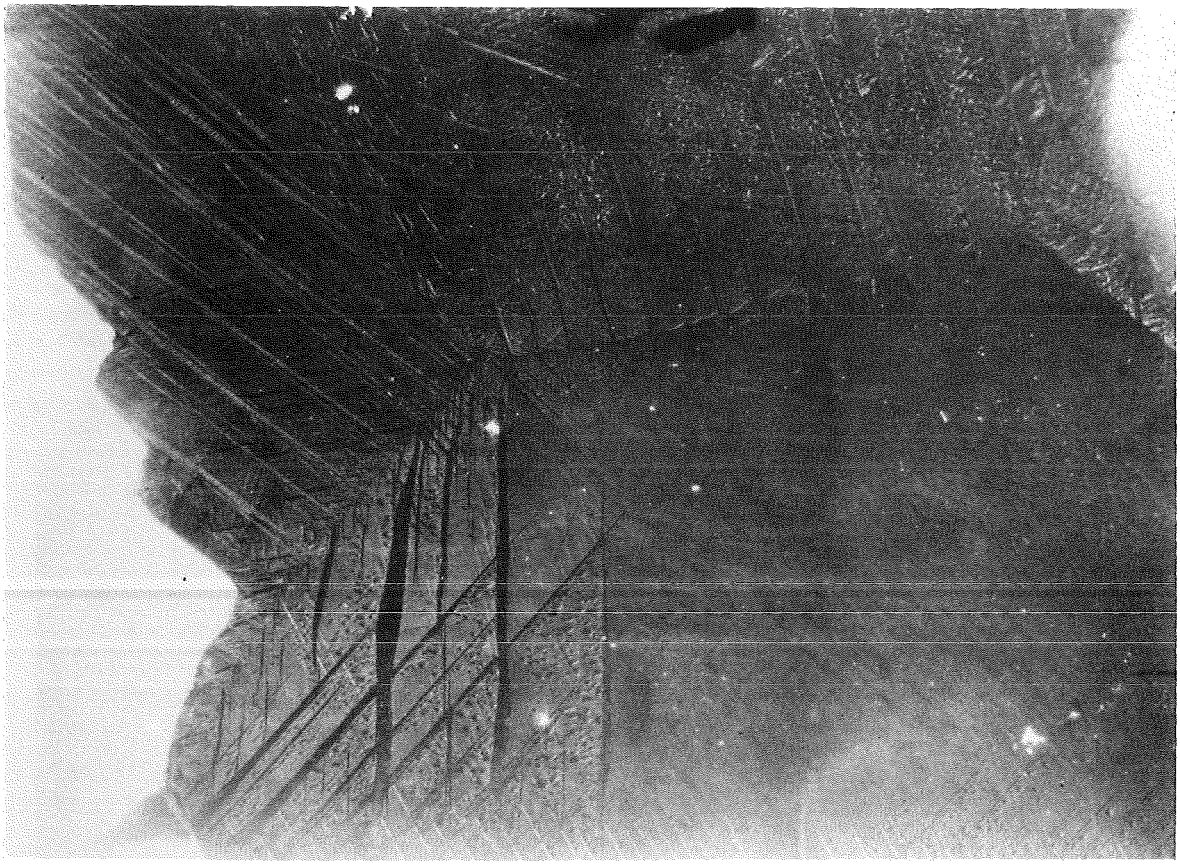

B x 100

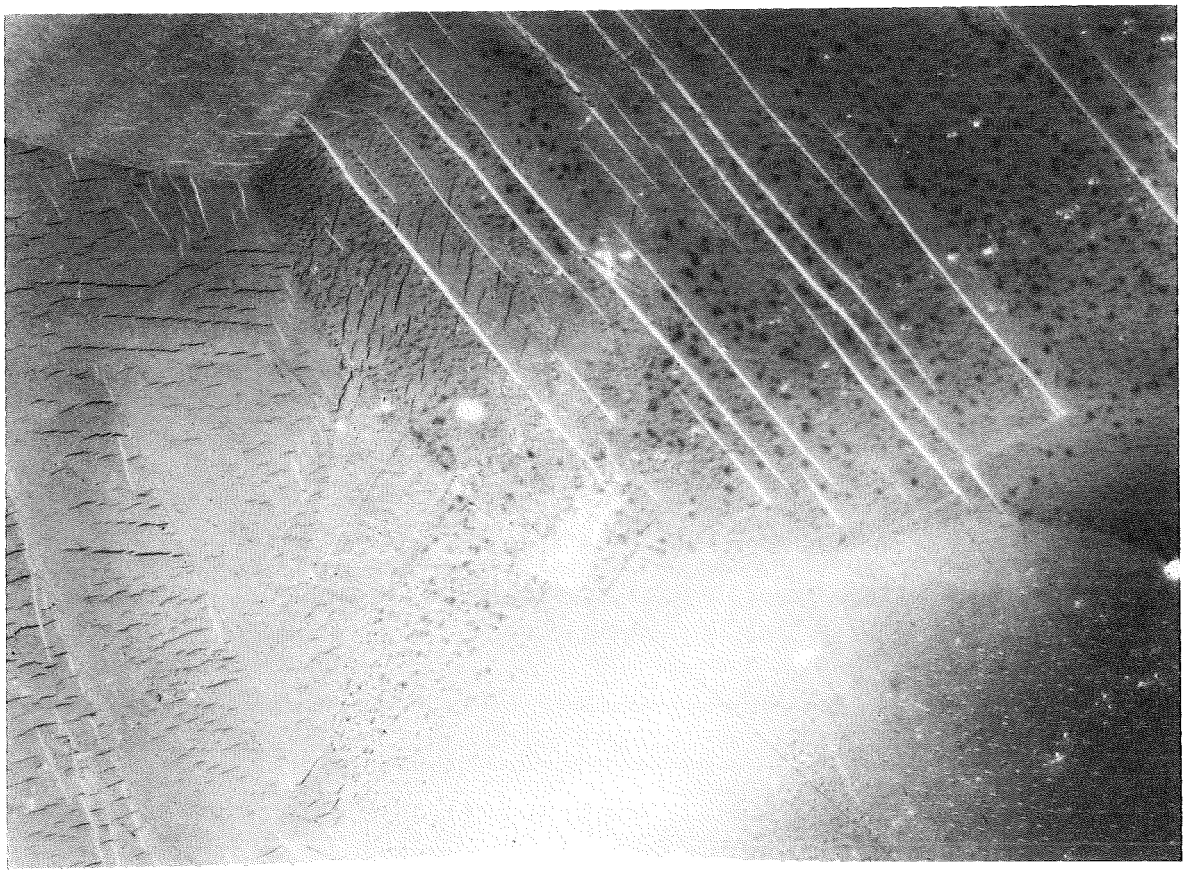

M x 100

(f) PHOTO F.0.9 PROBE 7-D T = -193°C

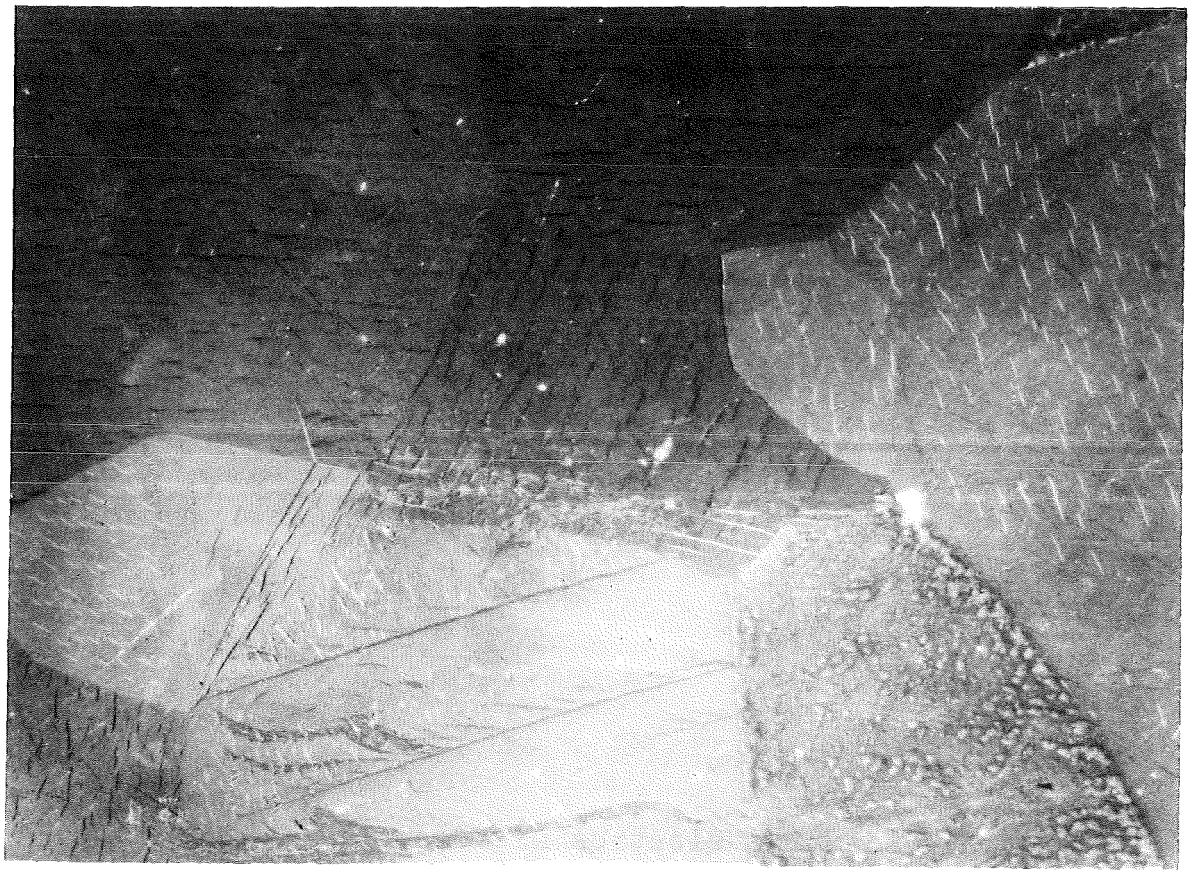

M x 100

(f) PHOTO F.O.9 PROBE 7-D T = -193°C

Fig. 13 Scanning electron microscopy
(a) Sample tested at T = 100°C
(b) " " " T = 100°C
(c) " " " T = 50°C
(d) " " " T = 50°C
(e) " " " T = -54°C
(f) " " " T =-101°C
(g) " " " T =-101°C
(h) " " " T =-101°C
(i) " " " T =-193°C
(j) " " " T =-193°C

PROBE № 2-D T: 100ºC
(a) 1 M.E.B. x 500

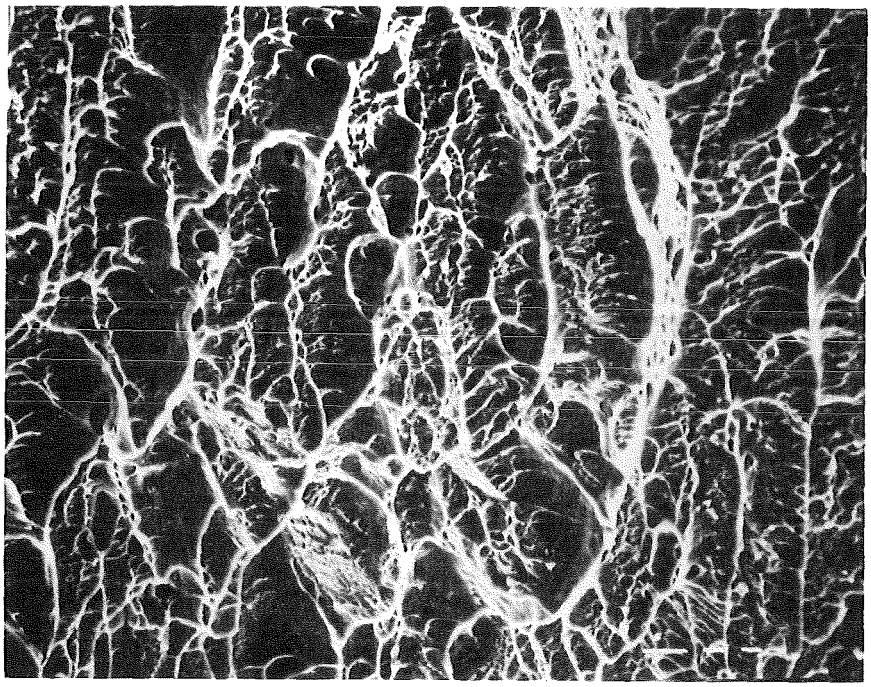

PROBE № 2-D T: 100ºC
(b) 2 M.E.B. x 500

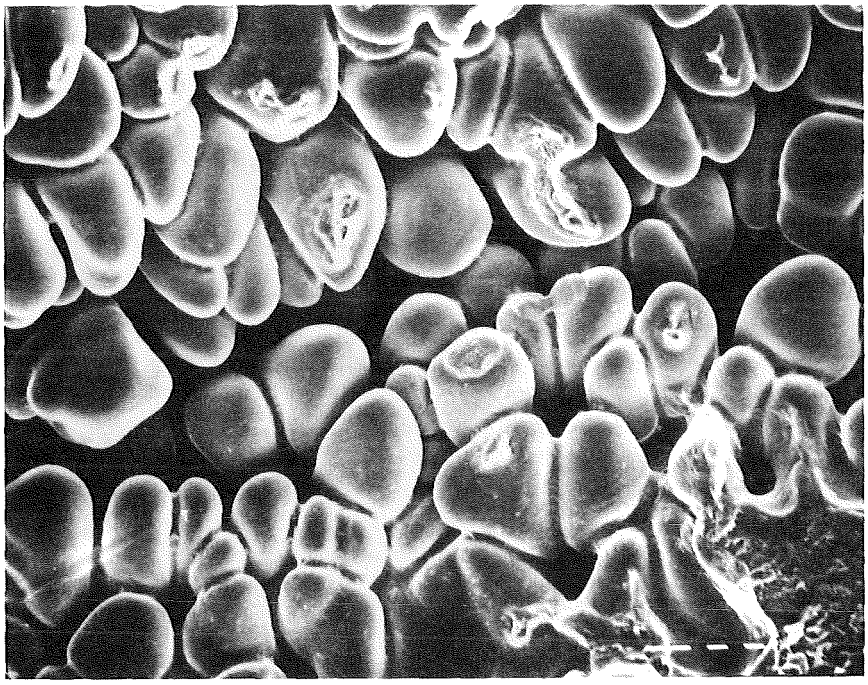

PROBE № 8-D T: 50ºC
(c) 3 M.E.B. x 500

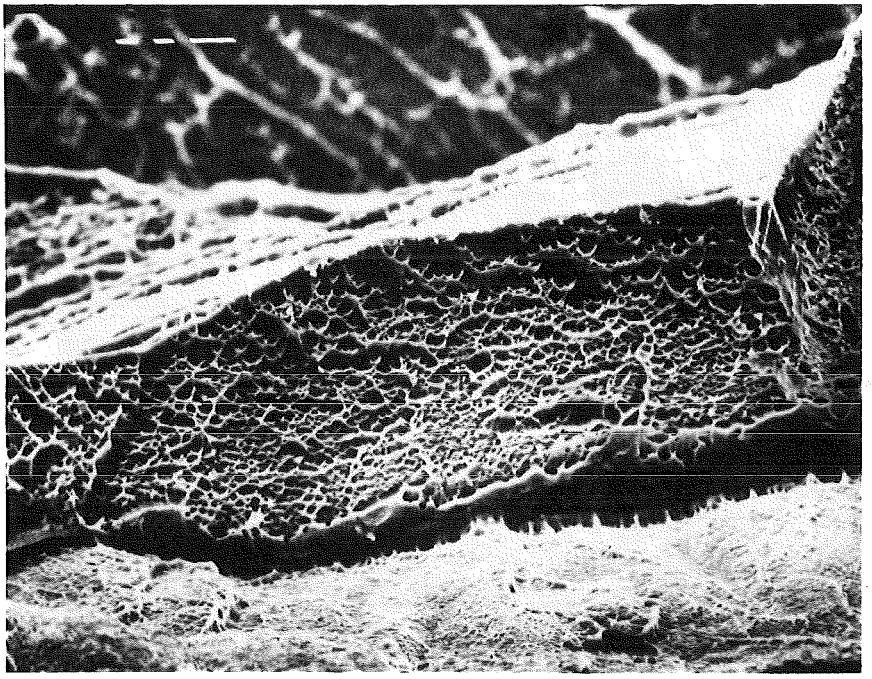

PROBE № 8-D T: 50ºC
(d) 4 M.E.B. x 200

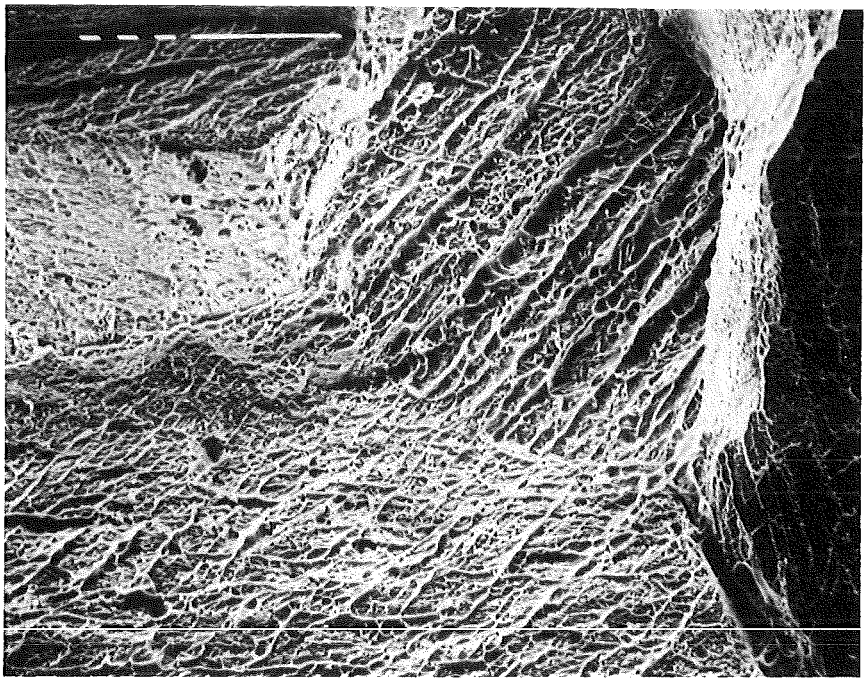

PROBE № 1-D T:-54°C
(e) 5 M.E.B. x 300

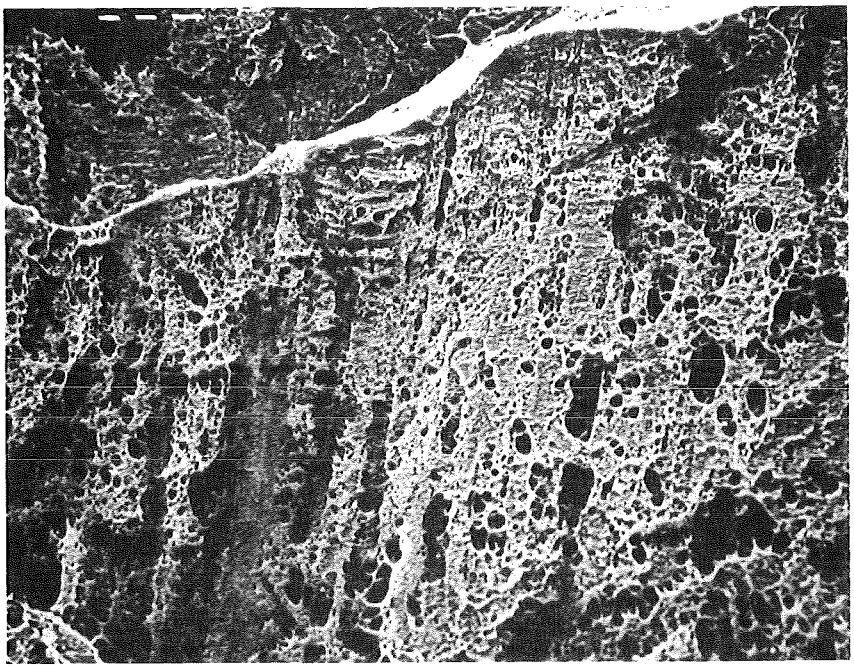

PROBE № 6 T:-101°C
(f) 6 M.E.B. x 500

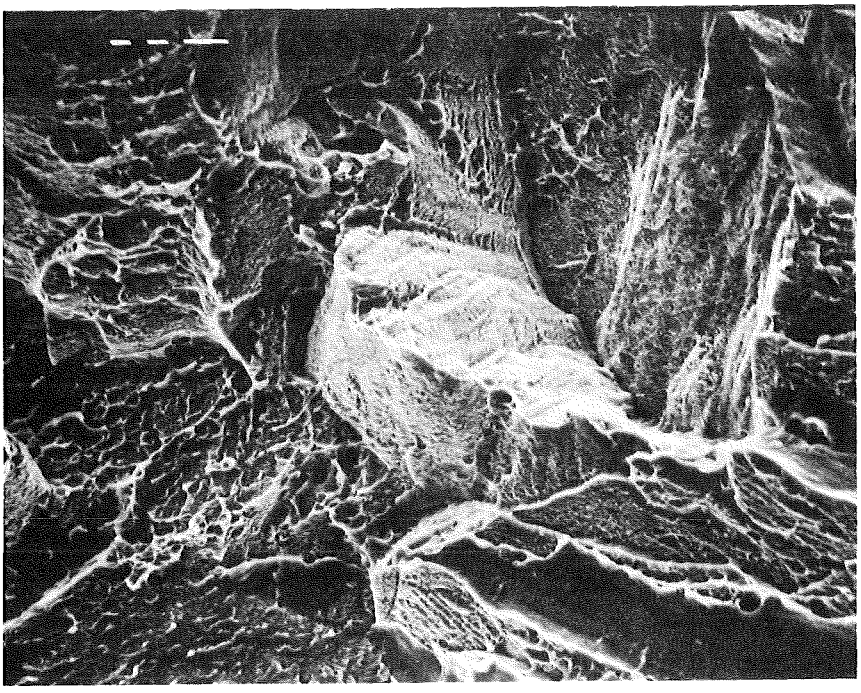

PROBE № 6 T:-101ºC
(g) 7 M.E.B. x 500

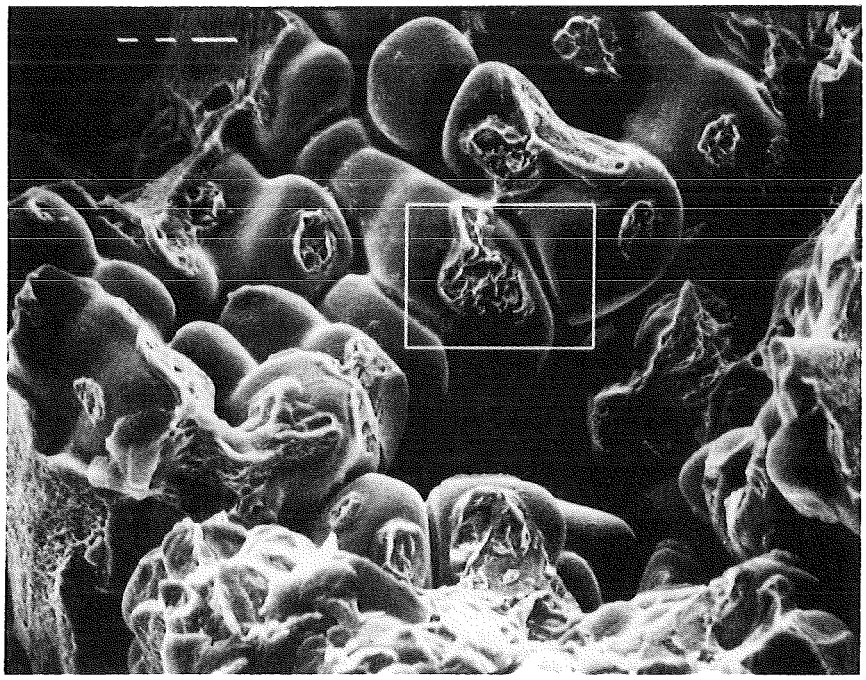

PROBE № 6 T:-101ºC
(h) 8 M.E.B. x 3000

PROBE № 7 T:-193ºC
(i) 9 M.E.B. x50

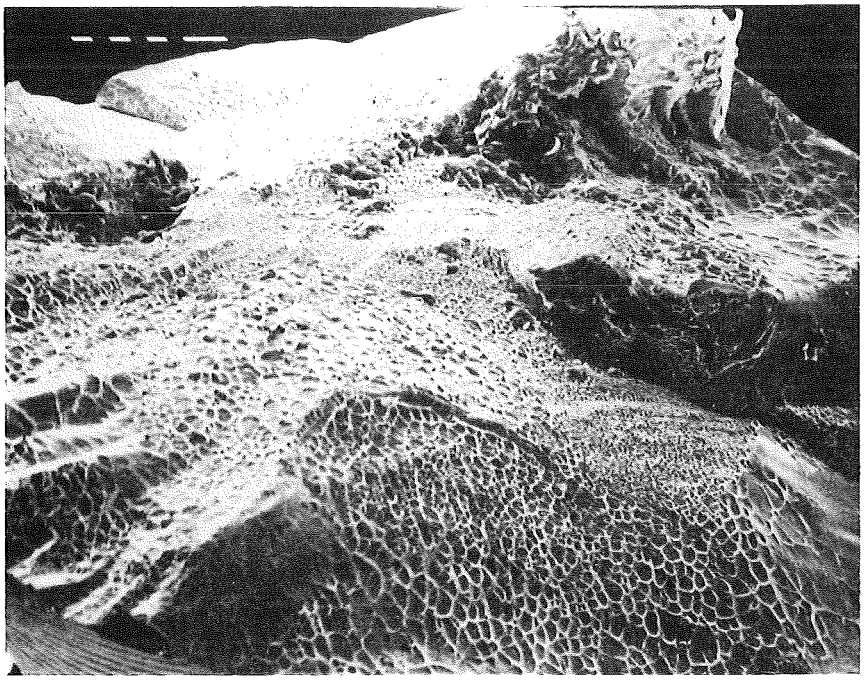

PROBE № 7 T:-193ºC
(j) 10 M.E.B. x 500

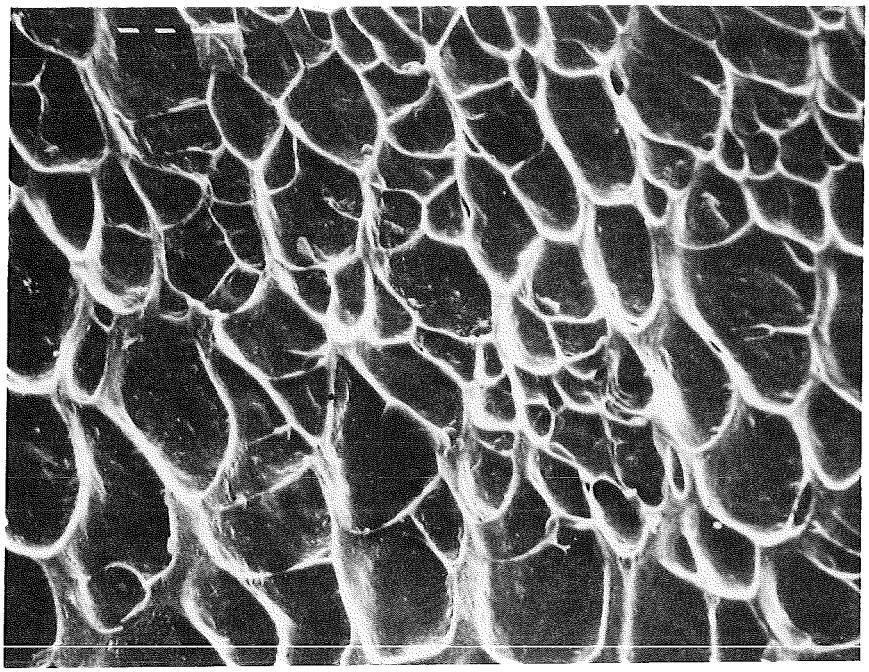

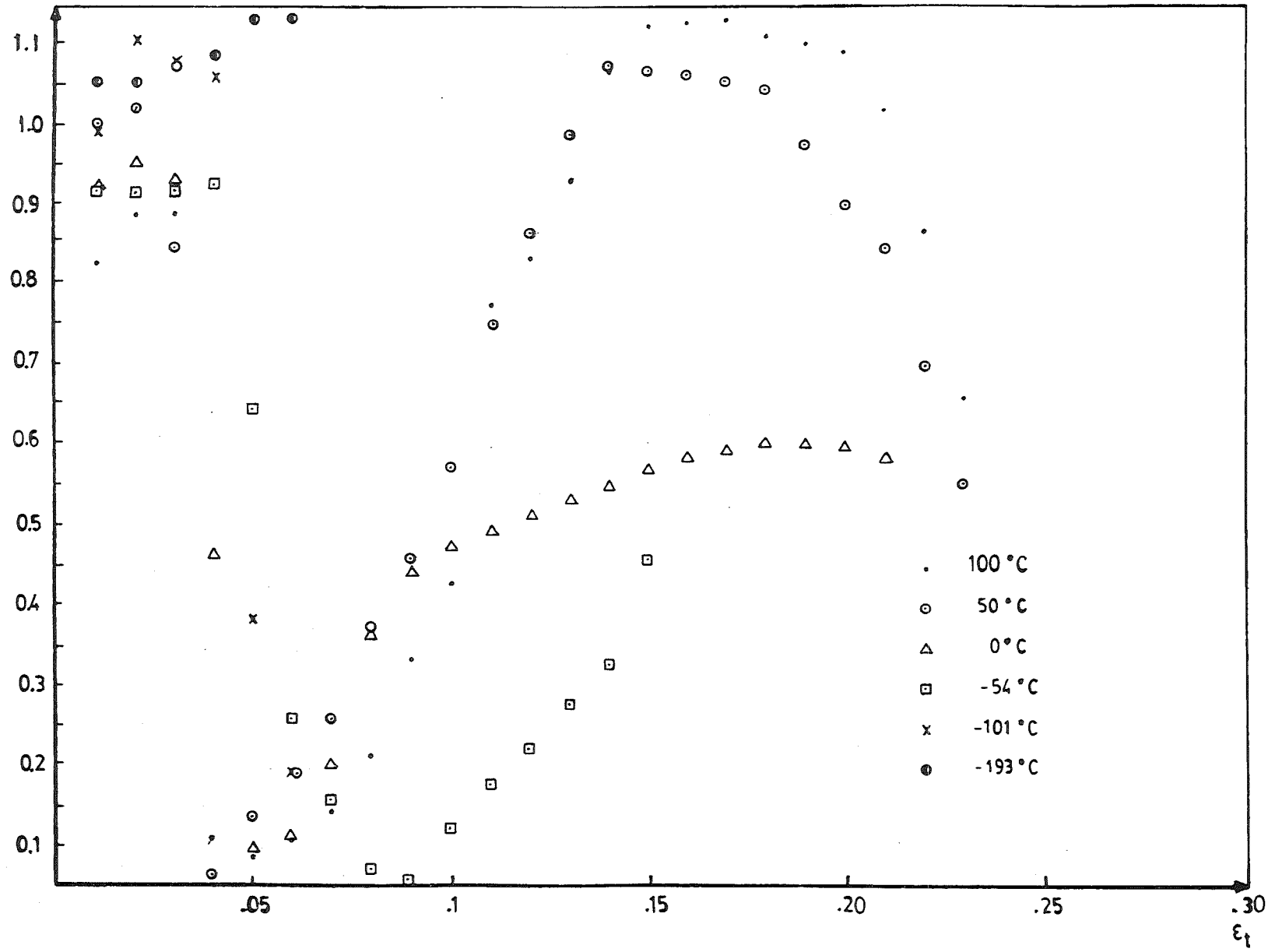

Fig. 14 Hardening coefficient n versus true plastic deformation ε_t, for the six tension tests.

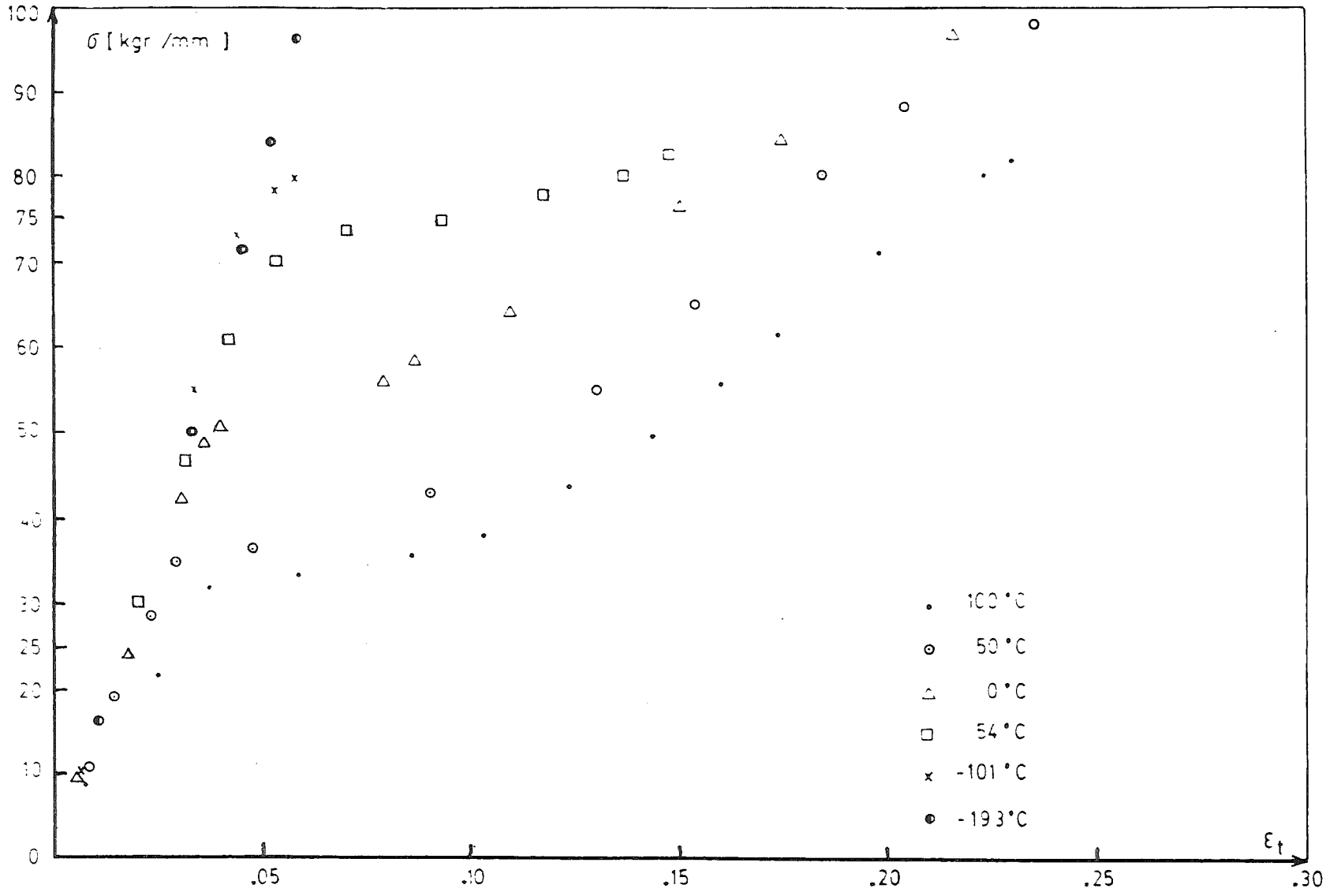

Fig. 15 True stress versus true plastic deformation, for the six tension tests.